https://doi.org/10.5194/bg-2019-462
Preprint. Discussion started: 7 January 2020

Biogeosciences Discussions

Particulate Rare Earth Element behavior in the North Atlantic (GEOVIDE cruise)

Marion Lagarde[1], Nolwenn Lemaitre[2], Hélène Planquette[3], Mélanie Grenier[1], Moustafa Belhadj[1], Pascale Lherminier[4], Catherine Jeandel[1]

[1] LEGOS, University of Toulouse, CNRS, CNES, IRD, UPS, Toulouse, 31400, France
[2] ETH, Zurich, IGP, Zurich, Switzerland
[3] LEMAR, University of Brest, CNRS, IRD, Ifremer, Plouzané, 29280, France
[4] LOPS, Ifremer,CNRS,IRD,UBO, Ifremer, Plouzané, 29280, France

Correspondence to: Marion Lagarde (marion.lagarde@legos.obs-mip.fr)

Abstract. Particulate concentrations of the fourteen Rare Earth Elements (PREE), yttrium and 232-thorium have been measured in two hundred samples collected in the epipelagic (ca 0-200 m) and the mesopelagic (ca 200-1000 m) zones of the North Atlantic, during the GEOVIDE cruise (May/June 2014, R/V Pourquoi Pas ?, GEOTRACES GA01). Particulate cerium (PCe) concentrations vary from 0.2 pmol.L^{-1} to 16 pmol.L^{-1}, particulate neodymium (PNd) ones from 0.09 pmol.L^{-1} to 6.1 pmol.L-1 and particulate ytterbium (PYb) ones from 0.01 pmol.L^{-1} to 0.5 pmol.L^{-1}. PREE concentrations are higher close to the Iberian margin and on the Greenland shelf, where PREE concentrations normalized to Post Archean Australian Shale (PAAS) display a positive Ce anomaly between 0.3 and 3, and a light REE (LREE) enrichment compared to heavy REE (HREE) illustrated by high PNd_N/PYb_N ratios (normalized to PAAS). The lithogenic fraction of the particulate REE concentration is closely related to the margin morphology and the hydrodynamic context: off the Iberian margin, up to 100% of the PREEs are lithogenic and this lithogenic input spreads westward along isopycnals as intermediate nepheloid layers (INL) up to 1700 km away. Lithogenic inputs are also observed along the Greenland and Newfoundland margins, although the circulation stacks them along the coasts. PREE distributions are also controlled by the biological uptake in the surface layers and remineralization processes deeper. Low surface concentrations and some normalized REE patterns displaying a negative Ce anomaly and HREE enrichment indicate freshly formed biogenic particles. A significant relationship between biogenic silica (BSi) and PHREE is also observed in the diatom blooms occurring in the Labrador and Irminger seas. PHo/PY ratio was calculated in order to identify processes independent of the ionic radius. However, we could not firmly assess the role of the iron hydroxides in the scavenging prates of these elements.

1 Introduction

Marine particles are the main way to transfer chemical species to the deep ocean together with the convection of water masses. Particles are abundant in the upper ocean, where dust inputs or massive blooms occur (up to 1000 µg.$L^{-1)}$, but their concentration decrease with depth (5 to 60 µg.L^{-1} on average in the subsurface and deep ocean, (McCave and Hall, 2002; Stemmann et al., 2002). However, particles are up to 1000 times more concentrated in elements than the dissolved phase (Lam

https://doi.org/10.5194/bg-2019-462
Preprint. Discussion started: 7 January 2020

et al., 2015), and especially in trace elements. For example, in the subpolar North Atlantic (GEOTRACES GA01 cruise, the section studied here), particulate Fe (PFe) concentration can reach 50 nmol.L^{-1} when dissolved Fe (DFe) does not exceed 2.5 nmol.L^{-1} (Gourain et al., 2019; Menzel Barraqueta et al., 2018; Tonnard et al., 2018). The size spectra between the particulate and the dissolved phase is continuous and the separation between both pools is operational, depending on the porosity of the filters used to discriminate the two phases, usually 0.4 µm (Planquette and Sherrell, 2012). Concentrations then depend on the choice of this limit, even if the vertical flux is mostly due to the large, dense, sinking particles, in opposition to the smaller and less dense particles that are in suspension in the water column. However, these small suspended particles represent over 80% of the total particle mass (Lam et al., 2015 and references therein). In addition, their higher surface to volume ratios make suspended particles the main drivers of dissolved-particulate exchanges.

In the ocean, three main sources of particles are distinguishable. The first one is lithogenic, with inputs from the rivers, dust deposits, ice melting and resuspension of deposited sediments. The second one is biogenic, and related to the production of fresh organic matter by photosynthetic activity followed by zooplankton grazing, and the following life cycle. The last one consists in authigenic processes such as red clay, oxides and hydroxides precipitation and formation. All these sources and processes lead to a very heterogeneous pool, in time, space and composition, evolving throughout their stay in the ocean and control the density of particles and consequently their fate in the water column. Then, exchanges between the particle and dissolved phases determine the chemistry of seawater and the residence time of the chemical species. They also determine the transfer rate of elements such as carbon and micro-nutrients between the upper layers and the deep ocean, where they are stored for times going from the global circulation scale (500 – 1000 years) to geological ones.

Oceanic tracers such as rare earth elements (REE) are truly adapted to the study of these exchanges (Jeandel et al., 1995; Kuss et al., 2001; Tachikawa et al., 1999). Physical and geochemical processes such as aggregation-disaggregation, dissolution, complexation, sorption, mineralization and scavenging lead to a fractionation along the REE series, depending on their origin and intensity. Thus, measuring the distribution of REEs between the solid and dissolved phases can help tracing and quantifying these processes.

The North Atlantic is a key region of the global ocean, as it is the highest oceanic sink of anthropogenic CO_2 (Khatiwala et al., 2013). Indeed, it is together i) a major place of deep water formation, mainly by convection, which drives the Atlantic meridional overturning circulation (AMOC), and ii) a productive area, representing up to 18% of the global oceanic primary production (Sanders et al., 2014).

In this context, we present the first basin scale section of PREE concentrations and fractionation patterns obtained for suspended particles collected in the North Atlantic (SPNA), along the GEOVIDE section (GA01 GEOTRACES cruise), from the surface to 1500 m. We will specifically discuss processes affecting the PREE distribution such as lithogenic inputs from the margins, influence of biological activity and the role of ionic radius on their fate in the water column.

https://doi.org/10.5194/bg-2019-462
Preprint. Discussion started: 7 January 2020


Biogeosciences Discussions

2 Methods

2.1 Study area: hydrographical and biogeochemical context

Samples have been collected in the epipelagic and mesopelagic zones (0 m – 1500 m) during the GEOVIDE cruise (16th of May 2014 to 30th of June 2014, R/V Pourquoi Pas ?) along the transect presented in Fig. 1. This figure also presents the main surface currents, as described in details (Zunino et al., 2017) and (García-Ibáñez et al., 2018), together with the three main biogeochemical provinces identified by Longhurst (1995) and described in details by Lemaitre et al. (2018). The position of the stations where PREEs were sampled (Fig. 1) were chosen to be representative of the diversity of biogeochemical provinces and water masses (Fig. 2).

Warm and salty waters coming from the tropical Atlantic are advected toward the Arctic by the North Atlantic Current (NAC, see Table 1 for abbreviations list). In response to air-sea exchanges and mixing with polar waters, surface waters become colder and fresher, but more importantly, denser. They tend thus to mix with underlying waters, particularly during convecting events triggered by storms. In the Nordic Seas (between 65°N and 80°N), the water column can be ventilated down to the bottom, while convection never exceeds 2000 m in the subpolar gyre. The freshly formed deep water then returns southward mainly via western boundary currents.

The North Atlantic Subtropical (NAST) province is characterized by warm and salty waters (García-Ibáñez et al., 2018; Longhurst, 1995; Reygondeau et al., 2018; Zunino et al., 2017). This province is depleted in nutrients, yet under influence of margin inputs, displayed a declining bloom of cyanobacteria during the cruise (Lemaitre et al., 2018). Stations #1 and #13 were sampled in the NAST. The North Atlantic Drift region (NADR) is located between the NAST and the Reykjanes ridge, with higher nutrient concentrations than in the NAST (Longhurst, 1995). A strong bloom of coccolithophorids, with a maximum intensity in the Icelandic basin, occurred during the cruise, generating the highest primary production rate observed on GEOVIDE (1740 molC.m^{-2}.d^{-1}, station #26, Fonseca-Batista et al., 2019) and high carbon export (up to 80 molC.m^{-2}.d^{-1}, station #32, Lemaitre et al., 2018). Four open ocean stations were sampled in this province: in the northern branch of the NAC (station #21), at the Subpolar front (station #26), in the northern branch of the NAC (station #32) and on the Reykjanes Ridge (station #38).

West of the Reykjanes Ridge, the Irminger and Labrador Seas (Fig. 1) are rich in nutrients, and belong to the Arctic region (ARCT). Large blooms of diatoms occurred in this area, which a maximum intensity at the end of May, in other words three weeks before GEOVIDE sampling in the Labrador Sea and one month before the sampling in the Irminger Sea. The western part of the ARCT region is under the influence of the Newfoundland margin. In this province, station #44 was sampled in the middle of the gyre of the Irminger Sea, station #51 in the EGCC and station #53 on the Greenland shelf. In the Labrador Sea, station #64 is in the West Greenland Current (the continuity of the EGCC after it passed Cape Farewell) and station #69 is in the area of formation of LSW, where strong convection events occurred the winter before GEOVIDE (García-Ibáñez et al., 2018; de Jong and de Steur, 2016). Westward, the station #77 is close to the Newfoundland margin (ca 300 km).

https://doi.org/10.5194/bg-2019-462
Preprint. Discussion started: 7 January 2020

2.2 Sampling at sea

Two sampling systems have been deployed during GEOVIDE to collect suspended particles: a standard CTD rosette equipped with 12 L Niskin bottles and a clean CTD rosette equipped with 12 L GO-FLO bottles. The standard rosette was used to collect samples dedicated to the concentration analyses of dissolved and particulate barium in excess (Ba_{xs}), dissolved and particulate REEs (including Nd isotopic composition) as well as ancillary parameter analyses. Ba_{xs} and PREE chemical treatment and analyses were conducted on the same samples: Ba_{xs} was first measured at the Royal Museum for Central Africa (Tervuren, Belgium), then PREEs were later analyzed at LEGOS (Toulouse, France; this work). Ba and ^{232}Th concentrations were measured at both places, allowing us to compare our procedures. Regarding the samples collected with the clean rosette, Ba, ^{232}Th and Y (with the latter belonging to REEs, named YREEs when Y is included) were also measured. Ba and ^{232}Th were used to compare the data obtained with the standard and clean rosette procedures (as done for Ba_{xs} by Lemaitre et al., 2018, with comparable results: r^2= 0.61, p <0.01, Fig. S1 in supplementary) distinguishable by the sampling systems, filtration method, chemistry performed on filters and analysis. The comparison of Y concentrations from the two procedures validated the use of our standard rosette to sample YREEs, less prone to contamination than trace metals, as shown by van de Flierdt et al. (2012).

Sampling method and sample preparation for water collection with the standard rosette for Ba_{xs} and PYREE analyses described here follow those of Lemaitre et al. (2018). Sampling was focused on the epipelagic and mesopelagic zones (0 m – 1500 m). On board, four to eight liters were filtered using clean slightly pressurized containers. Bottles were shaken three times as recommended in the GEOTRACES cookbook, to avoid the loss of particles by sticking to the walls or settling at the bottom of the bottle. Seawater was then poured in the Perspex containers at the base of which polycarbonate filters of 0.4 µm porosity (Nuclepore®, 47 mm or 90 mm of diameter) were mounted. After sample filtration, the container was rinsed with ≤5 mL of ultra-pure water (Milli-Q; 18.2 MΩ.cm) to remove the maximum of sea salt deposited on the membranes. Finally, filters were removed using plastic tweezers and were dried under a laminar flow hood at ambient temperature before being stored in clean petri dishes.

Regarding samples collected with the clean rosette, sampling method and samples preparation are described in Gourain et al. (2019).

2.3 Sample preparation and analysis

Filters were first cut in two parts using a ceramic blade. One half was archived, while the other half was placed in a clean Teflon vial (Savillex®). The filter was then digested with a strong acid solution made of 1.5 mL HCl, 1 mL HNO3 and 0.5 mL HF, all concentrated (Merck® Suprapur Grades). Vials were subsequently left on hot plates at 90°C overnight.

The PREE concentrations were measured on 2 mL of the archived solutions, which were placed in clean 5 mL polypropylene tubes and doped with a solution containing In and Re (ca 100 ppt of both tracers) in order to correct matrix effects and sensitivity shifts during analysis. In addition to REEs, Y, Ba and ^{232}Th concentrations were measured in the same leaching

https://doi.org/10.5194/bg-2019-462
Preprint. Discussion started: 7 January 2020

solution. Analyses were performed at the Observatoire Midi Pyrénées (Toulouse, France) using a high-resolution inductively coupled plasma mass spectrometer (SF-ICPMS, Element XR, Thermo Fischer Scientific®) coupled to a desolvating nebulizer (Aridus II, CETAC Technologies®) to minimize oxides and hydroxides production rates and thus (hydr)oxides interferences (Aries et al., 2000). Oxide production rates were determined at the beginning and the end of every session using a mono-elementary Ce solution (CeO<0.03%). Other REE (hydr)oxides rates were then determined using the constant proportionality factor between them (Aries et al., 2000), previously determined with the same analytical configuration. Interferences represent 0.001% to 1% of the signal except for Eu (0.3% to 10%).

A five points calibration curve was established with a multi elemental standard at the beginning, the middle and the end of the analysis, while a standard solution concentrated with 20.10^{-12} $g.g^{-1}$ of REE was measured every 5 samples. The certified reference material SLRS-5 (NRC Canada) was systematically analyzed with the samples and their concentrations are within the error bar of the consensual values published by Yeghisheyan et al. 2013, with a smaller error (see Figure S1 in supplementary). Reproducibility was assessed by measuring two or three times several samples from the same leaching solution, and varied from 0% to 20%, like the error.

Procedural blanks have been estimated by conducting the chemistry on clean, unused filters. The average chemical blank (n= 8) represents 0.01% to 5% of the sample concentrations, except for Y and Lu for which the contribution of the blank was generally higher (between 1% and 30%).

Uncertainty of each concentration, estimated from error propagation was between 20% and 30% (and can be up to 40% for Eu) of the concentration. In addition to the mass spectrometry standard deviation the other sources contributing to the final error bar of the concentrations are: the proportion of filter analyzed, the volume of leachate and the volume taken in the archive for the analysis. For details on errors, see Fig. S2 in supplementary.

Thus the hypothesis of homogeneity is assumed, in the light of the apparent consistency of suspended particles on filters.

The same digest solutions were also analysed at the Royal Museum for Central Africa (Tervuren, Belgium) mainly for determining Ba and some other element concentrations, including ^{232}Th. It was conducted using an inductively coupled plasma quadrupole mass spectrometer (ICP-QMS; X Series 2 Thermo Fischer®). Ba, Y and ^{232}Th were also measured in clean rosette samples. The digestion procedure and analytical method are detailed in Gourain et al. (2019). Concentrations of Ba and ^{232}Th are consistent between the analysis conducted in Brest and the PREE analysis in Toulouse. “Toulouse” Ba concentrations vs. “Tervuren” Ba concentrations give a regression slope of 0.87 (r^2=0.90, n=198). For ^{232}Th, “Toulouse” concentrations vs. “Tervuren” concentrations give a slope of 1.05 (r^2=0.98, n=198), which is also very comparable. Ba and Y analyses were used to compare the clean rosette and standard rosette procedures. Consistent Ba concentrations were found when compared to the results of Lemaitre et al. (2018; r^2=0.61, n=66). Y concentrations measured in Toulouse on samples collected with the standard rosette match the concentrations obtained in Brest on the clean samples, with a regression slope of 0.93 (r^2=0.82, n=78 points at same depths). Thus both procedures are suitable for PREE analysis. In addition, these validations allow us to discuss the PREE concentrations with the trace metal ones from Gourain et al. (2019).

https://doi.org/10.5194/bg-2019-462
Preprint. Discussion started: 7 January 2020

3 Results

The data set of PYREE, PBa and $P^{232}Th$ concentrations is compiled in Table 2. For sake of clarity, we only displayed PCe, PNd and PYb concentrations (Fig. 2 and 3), these three REEs representing the light REEs (Nd), heavy REEs (Yb) and a specific behavior (Ce). LREEs and HREEs are supposed to react to different processes during dissolved-particulate exchanges. Ce has a IV oxidation state in addition to the III oxidation state common to all REEs and its oxidation onto particles prevent desorption. The Ce (III)/Ce(IV) distribution is therefore a proxy of redox and desorption processes.

PCe (Fig. 2) concentrations are higher than PNd (Fig. 3 and B) concentrations, which are higher than PYb concentrations (Fig. 3 C and D), in agreement with their respective natural abundance and reactivity.

3.1 Cerium

Particulate Ce concentrations (PCe, Fig. 2) vary between 0.2 pmol.L^{-1} (station #64) and 16.3 pmol.L-1 (station #32; Fig. 2). They are higher close to the Iberian margin (station #1: 1 pmol.L-1 < PCe < 9.4 pmol.L^{-1}) and on the Greenland shelf (station #53: 5.7 pmol.L^{-1} < PCe < 14.6 pmol.L^{-1}). In the NAST (for station #13) and the NADR regions, vertical profiles present a surface or subsurface maximum at all stations. Below 200 m depth, PCe concentrations decrease and reach a value of 2 pmol.L^{-1} in the mesopelagic zone. PCe concentrations are higher to the east of the polar front (stations #13 and #21) compared to the west (stations #26, #32 and #38). A second maximum is observed at greater depth at station #13 and in the NADR region (except close to the subarctic front, at station #26). In the ARCT region, surface PCe concentrations are lower and increase at the bottom of the epipelagic zone for all open-sea stations (PCe > 1 pmol.L^{-1}). Maximum concentrations are observed at the bottom of the epipelagic zone at stations #44, #64 and #69. PCe concentrations are more variable in the mesopelagic zone of the ARCT region than in the NADR region, and higher than the ones observed at the surface except at station #69 where they are about within the same range (1 pmol.L^{-1} < PCe < 2 pmol.L^{-1}). PCe profiles differ from that of PNd and PYb at two stations only: station #38, where peaks of PCe are observed at 100 m and 800 m, that are not observed for the other PREE profiles; station #44, where PCe concentrations are more variable in the epipelagic zone than PNd and PYb, with maxima at 120 m and 160 m that are not observed for other PREEs.

3.2 Neodymium

As for PCe (and other PREEs, see supplementary information), PNd concentrations are the highest close to the Portugal and Greenland margins with values up to 4.5 pmol.L^{-1} in the upper 100 m (Fig. 3 a and B). Concentrations decrease as the distance to margins increases, as seen at stations #13 where PNd hardly reaches 1 pmol.L^{-1}. Low PNd values were also measured at station #77, although this station is relatively close to the Newfoundland margin, but located out of the continental shelf.

https://doi.org/10.5194/bg-2019-462
Preprint. Discussion started: 7 January 2020

3.3 Ytterbium

Distributions of PNd and PYb (Fig. 3) differ on several points: three stations (#13, #44 and #69) display a maximum in subsurface for PYb that is not observed for PNd, whereas a local maximum in PNd is identified at 160 m at stations #64 and #69, but not for PYb. In the open ocean, at stations #21, #26, #32 and #38, concentrations are higher in the surface layer (from 0 m to 200 m). The highest concentrations were determined in the NADR region, which was the most productive during the cruise (Fonseca-Batista, 2018). Concentrations then decrease with depth to become constant, except at station #38 where they increase again in the mesopelagic zone. In the ARCT region, surface concentrations of PNd are lower at 100 m compared to 250 m, similar to station #1 while the contrary is observed in the NADR region.

3.4 PNd_N/PYb_N ratios

To highlight a possible fractionation between LREE and HREE, the PNd_N/PYb_N ratio is calculated from concentrations normalized to PAAS, in order to get rid of the natural abundance effect of the REEs. Results are presented in Fig. 4, interpolated along the section. This ratio presents a high variability, changing from 0.01 to 4.3. Higher ratios (> 1) are observed along the margins, decreasing as the distance to the coast increases. PNd_N/PYb_N is lower at the surface (< 0.7) except at stations #1, #38 and #53, and increases in the subsurface layers ($0.7 < PNd_N/PYb_N < 1$) in the open ocean. The strongest ratio value is observed in the core of the epipelagic zone at station #21 (Fig. 4C), where high concentrations of PLa, PCe, PPr and PNd are also observed. However, for other stations with a similar enrichment, no high PNd_N/PYb_N ratio are observed.

4 Discussion

4.1 Comparison with other studies

PREE data in suspended particles are very scarce in the literature. To our knowledge, for the North Atlantic, only one other set of concentrations was published by Kuss et al. (2001), who measured PREEs in samples centrifuged from several m^3 of water at a depth of 7 m, collected along the 20°W meridian between 30°N and 60°N. These authors observed PCe concentrations ranging between 0.2 $pmol.L^{-1}$ and 4.9 $pmol.L^{-1}$ with higher concentrations close to the margins especially near the European one, consistent with our data. Their PNd concentrations of about 0.5 $pmol.L^{-1}$ to the east of the NADR are also consistent with ours. PNd and PYb concentrations reported by Tachikawa et al. (1999) at a station located in a mesotrophic zone of the north-east tropical Atlantic, directly influenced by Saharan dust (6 $g.m^{-2}.yr^{-1}$ to 15 $g.m^{-2}.yr^{-1}$,Rea, 1994), are higher than those reported here (PNd = 2.6 $pmol.L^{-1}$ and PYb= 0.94 $pmol.L^{-1}$ at 10 m). Contrastingly, these authors observed lower concentrations than ours at the oligotrophic site of their study, where the dust flux is lower than at the mesotrophic site (4-5 $g.m^{-2}.yr^{-1}$, Rea, 1994) but higher than that found during the GEOVIDE cruise (2 $ng.m^{-3}$ to 500 $ng.m^{-3}$, Shelley et al., 2017). However, these author's PCe concentrations are similar to those reported in this study, and that for both the mesotrophic and

https://doi.org/10.5194/bg-2019-462
Preprint. Discussion started: 7 January 2020

oligotrophic sites. The difference of concentrations observed for the other PREEs can be explained by the high particle concentrations characterizing the compared to the tropical one, even if dust inputs are higher on the later (Gehlen et al., 2006). PREE are found both in the lithogenic and authigenic phases of the particles. Schematically, particles are often represented with a "lithogenic core" coated by authigenic material (Bayon et al., 2004; Sholkovitz et al., 1994). The lithogenic has an external origin, product of the continental weathering transported by the winds or discharged by the rivers on the margins. The authigenic phase is of internal origin, major phases being biogenic matter (particulate organic matter POM, biogenic silica BSi, calcium carbonate $CaCO_3$) and metal oxides and hydroxides such as MnO_2 and $Fe(OH)_3$. REEs in the authigenic phase are scavenged by organic coatings and/or iron and manganese oxides and hydroxides that are known to be the main carrier of REEs, scavenged by adsorption during their precipitation (Bau, 1999; Bau and Koschinsky, 2009). REEs could also be absorbed in inorganic planktonic tests ($CaCO_3$, Palmer, 1985 and BSi,Akagi, 2013) or biogenic byproducts as barite (Ba_{xs},Guichard et al., 1979). LREEs would be more sensitive to oxide phases of Fe and Mn, while HREEs, more soluble, could react preferentially with biogenic phases (Akagi, 2013; Bertram and Elderfield, 1992; Grenier, 2018; Pham et al., 2019). Their distribution coefficients are also varying with depth and the nature of the particle phases (Schijf et al., 2015).

Thus, differentiating the distribution of the REEs in the two phases allows us to estimate the fraction implied in scavenging processes by the authigenic phase, while the lithogenic one enables to picture continental inputs. The high PREE concentrations observed in Fig. 3 close to the Portugal margin and on the Greenland shelf suggest that particulate material is released by the margins to the water column. Lithogenic REE fraction can be quantified using conservative lithogenic tracers such as Al, Th or Ti (Gourain et al., 2019; Tachikawa et al., 1997). These authors used Al as a lithogenic tracer, but here we chose to use ^{232}Th. Indeed, the lithogenic fractions calculated from particulate Al (PAl) concentrations were often higher than 100% in surface waters close to the margins, revealing that a fraction of the total Pal is likely in the authigenic phase (Lerner et al., 2018; Van Beueskom et al., 1997). In addition, Al being more prone to contamination was sampled with the clean rosette (Gourain et al., 2019), while ^{232}Th used for calculation was measured in the same samples as PREEs, collected with the standard rosette. The concentration of the lithogenic PREE fraction in particles is calculated by multiplying the ^{232}Th concentration in a given sample by the ratio of the considered REE on ^{232}Th in the upper crust (Rudnick and Gao, 2014, Eq. (1)).

$$[\mathrm{REE_{litho}}] = [^{232}\mathrm{Th}] \times \left(\frac{[REE]}{[232Th]}\right)_{UCC} \quad (1)$$

$$\%REE_{litho} = \frac{[REE_{litho}]}{[REE]} \quad (2)$$

$$REE_{authi} = REE_{total} - REE_{litho} \quad (3)$$

These PREE lithogenic concentrations are then divided by the total PREE concentrations to obtain the percentage of particulate REE with a lithogenic origin (Eq. (2)). The authigenic concentrations are then obtained by subtraction of the lithogenic concentrations to the total concentrations (Eq. (3)).

https://doi.org/10.5194/bg-2019-462
Preprint. Discussion started: 7 January 2020

The percentage of lithogenic PNd along the section is represented in Fig. 5. Then we chose to represent the average value of the lithogenic fractions of the remaining PREEs for the LREE, excepted for PCe on one hand and for HREE on the other hand. Profiles of five selected stations (#1, #26, #51, #53 and #77) are shown in Fig. 5. These stations are representative of the three different distributions observed along the section. Error bars represent the standard deviation of the resulting averages, the contribution of the error on the concentrations being negligible compared to the laters. For some points at station #1 and at 160 m at stations #13 and #32, the calculated lithogenic proportion exceeds 100%, suggesting an excess of ^{232}Th in the particles, likely authigenic, or a difference between the adsorption kinetics of ^{232}Th and REE, as reported by Hayes et al. (2015). In these cases, we capped the lithogenic proportion to 100%.

PREE concentrations are normalized to Post-Archean Australian shale, PAAS (Rudnick and Gao, 2014). This normalization allows i) a better diagnostic of the fractionation between PREEs and ii) comparison with patterns in the literature. As shown by the flat PAAS-normalized patterns of the lithogenic fractions (Fig. S3 in supp. mat.), PAAS is a valuable reference to represent the lithogenic material. In addition, it does not present any significant difference in REE composition with shales and loess from Europe, North America and China (Rudnick and Gao, 2014). Normalization to atmospheric depositions has been put aside as these inputs were low during the cruise (Shelley et al., 2017) and normalization to dusts led to patterns depleted in Eu and Gd, and enriched in Tb, Dy, Ho and Er (data from Patey et al., 2015, on dusts collected close to Cape Verde; Fig. S3), less representative of lithogenic inputs than PAAS. Patterns normalized to PAAS are presented in Fig.5 for selected stations. To facilitate readability, patterns of each sample are averaged by layers displaying similar values. Error bars represent the standard deviation of the concentration series, the errors on PAAS concentrations being negligible compared to it. A REE pattern obtained in the Atlantic seawater at 12°S (Zheng et al., 2016) is also represented together with station #26 patterns, for comparison.

4.2 Lithogenic supply by the margins

The high concentrations of PREEs (Fig. 3) at stations #1 and #53 reflect lithogenic inputs from the margins. At these stations, the lithogenic PREE fractions range between 50% and 100%, the highest ones being observed at station #1 (Fig. 5). The relatively flat patterns displayed at these stations for total PREE indicate a weak fractionation of PREEs, with a little enrichment in LREEs due to their lower solubility compared to the HREEs. These maxima can be seen beyond the Subpolar Front until station #32, spreading along the isopycnals 27.05 and 27.4 over 2500 km from the Iberian margin (Fig. 6). Similar maxima have been reported by (Gourain et al., 2019, Fig. 6 B) for lithogenic PFe and PMn), lithogenic PMn being taken by these authors as tracer of sediment resuspension.

Above the Greenland shelf, at station #53, the proportion of lithogenic PREE is also high, only slightly lower than at station #1 (median contributions of 59% for PLREE and 83% for PHREE; Fig. 5). Unlike what is observed to the eastern end of the section, these lithogenic particles remain on the shelf and do not spread offshore. Except at the surface for LREE, the lithogenic proportion are lower than 50% at stations #51 and #64 in the Irminger Sea and in the Labrador Sea respectively. This containment of particles along the shelf is explained by the circulation. Indeed, the East Greenland Irminger Current (EGIC)

https://doi.org/10.5194/bg-2019-462
Preprint. Discussion started: 7 January 2020

285 is a strong narrow current bypassing Greenland along it shelf (23.4 ± 1.9 Sv, Daniault et al., 2016), likely preventing exchanges between the Irminger Subpolar Mode Water (IrSBPMW) and waters of the Greenland shelf, transported by the EGCC current which flows parallel to the coast (green and orange arrows around the Greenland southeastern tip in Fig. 1). Our observations are consistent with that of Lacan and Jeandel, 2005, who showed that the Nd isotopic signatures (εNd) of SPMW transported by the EGIC do not vary significantly along the Greenland shelf. In the same way, the lithogenic influence is moderate at 290 station #77, land-ocean exchanges being reduced due to the EGCC again (1.5 ± 0.2 Sv, Daniault et al., 2016). While the lithogenic fraction is still relatively high at this station (50% < REE_{litho} <80% below 150m), the fractionated patterns indicate that other processes are at play.

High lithogenic proportions are also observed at station #69 but not to the east of the Labrador Sea (station #64; Fig. 5). In contrast with the Iberian margin, no intermediate enriched layers are observed (Figs. 2 and 3) and the lithogenic fraction is less 295 important and remains roughly constant below 200 m at stations #51 (about 45%) and #77 (around 60%, Fig. 5). Normalized total concentrations display fractionated PREE patterns, underlining authigenic processes likely at play in this area.

Comparable lithogenic percentages have been reported by Garcia-Solsona et al. (2014) between South Africa and Antarctic, from 0% at the surface to 80% deeper, with higher lithogenic proportions for HREE than for LREE. Using PAl as a lithogenic tracer, Tachikawa et al. (1999) evaluated the lithogenic proportion to be between 50% and 80% at the different Eumeli sites 300 in the east tropical Atlantic.

Gourain et al. (2019) reported similar results than ours for PFe and PMn at the same stations along GEOVIDE. These authors observed strong lithogenic contribution from the Iberian margin spreading until station #32, lower contribution along the Newfoundland margin and no particular lithogenic contribution along the Greenland margin, in agreement with our observations. Using lithogenic PMn as a tracer of sediment resuspension, they observe that 100% of PMn is originating from 305 sediment resuspension at station #1 between 250 m and 1000 m (their Fig. 4). Interestingly, Le Roy et al. (comm. pers.) observed an unexpected maximum of ^{227}Ac activity at 500 m at stations #1 and #21, indicating a strong sediment source, again consistent with the PREE data. At station #13 at 200 m, however, no lithogenic maximum is identified. This could result from the compression of isopycnals, leading to the merging of the two maxima observed eastward (Fig. 4). Unfortunately, the different sampling resolutions for PREE and ^{227}Ac do not permit to further compare data between these tracers except at the 310 surface of station #1, where a maximum of ^{227}Ac is consistent from the lithogenic PREE signal.

These layers highly enriched in lithogenic particles could be attributed to the formation of intermediate nepheloid layers (INL) at 250 m and 500 m along the Iberian margin, similarly to those revealed slightly north by McCave and Hall (2002). A contribution of the Mediterranean Water (MW) to these high concentrations and lithogenic proportions cannot be excluded too, but the lack of data in the core of the MW (1000 m to 1500 m, García-Ibáñez et al., 2018) prevents us from further 315 investigations.

A highly energetic process is needed to enhance such strong resuspension of lithogenic matter. It may be due to the friction and energetic excitation of internal waves along the continental slope (Cacchione, 2002). Another source can be the erosion of the coast by the strong current (from 0.05 $m.s^{-1}$ to 0.1 $m.s^{-1}$) coming out from Gibraltar and flowing northward along the Iberian

https://doi.org/10.5194/bg-2019-462
Preprint. Discussion started: 7 January 2020

margin (Gourain et al., 2019; McCave and Hall, 2002; Zunino et al., 2017). Our observations could also result from a combination of both, with generation of internal waves south of station #1 generating sediment resuspension, those particles being advected northward by the current.

To sum up, margins can provide significant amounts of particulate lithogenic material to the ocean; nevertheless, occurrence and magnitude of these inputs are depending on the morphology of the margin and the hydrodynamical forcing, leading (or not) to nepheloid layer formations.

4.3 REE fractionation: Ce anomalies

Ce is the only REE having a (IV) oxidation state in the water column. When adsorbed onto particles together with other REEs, oxidation (biotic or abiotic) makes it less prone to desorption than other REEs, leading to Ce enrichment of the particulate phase (Byrne and Kim, 1990; Elderfield, 1988; Moffett, 1990, 1994; Tachikawa et al., 1999). This oxidation is thought to occur for authigenic Ce adsorbed on $Fe(OH)_3$ and MnO_2 (Bau, 1999; Bau et al., 1996). This PCe enrichment is commonly quantified by the ratio of the PCe concentration on the theoretical PCe concentration calculated using its neighbors PNd and PPr and expressed as Ce*, following Bolhar et al. (2004):

$$\frac{Ce}{Ce^*} = \frac{[Ce]}{2 * [Pr] - [Nd]} \quad (4)$$

In the present set of data, this ratio is always larger than one (positive anomaly) except at stations #26, #32, #51 and #77 between the surface and ca. 100 m, where PCe is depleted compared to other PREEs, as already discussed above. This surface minimum is followed by a pronounced (Ce/Ce*>3) positive anomaly down to 200 m. At greater depth, the anomaly is relatively higher in the NADR region compared to the NAST and ARCT regions.

These results indicate that Ce oxidation occurs after particles left the surface, leading to a subsurface maximum. At greater depths, remineralization rates are high in the ARCT region, moderate in the NAST region and low in the NADR region (Lemaitre et al., 2018). It is likely that lower remineralization rates conduct to higher net fluxes from the dissolved phase toward the particulate phase, associated with a strong and irreversible scavenging of Ce by adsorption and oxidation, while a fraction of the other trivalent REEs are released by desorption from the particles (Bau, 1999; Tachikawa et al., 1999). A stronger anomaly could also reflect higher particle concentrations offering higher surface reactive areas, but particle mass remains unknown at those depths and beam transmissiometry does not allow identifying higher particle concentrations.

To compare PCe to Mn and Fe (hydr)oxides, particulate $Fe(OH)_3$ and MnO_2 concentrations are calculated with the formula of Lam et al. (2017, Figure S6) using PMn, PFe and PAl data from Gourain et al. (2019). The observed decoupling between Ce anomaly and MnO_2 distributions indicates that more processes are at play than the biologically mediated oxidation that would lead to similar distributions of the two tracers (Moffett, 1990). Different complexation conditions between these two elements likely prevent the occurrence of a good correlation. The positive Ce anomaly is not observed when the residence time of particles is short, which is the case in the NADR and the ARCT regions where the export is strong (stations #51 and #77, Lemaitre et al., 2018). $CaCO_3$ formation can explain the observed negative anomalies at station #26 and #32 (Garcia-Solsona

https://doi.org/10.5194/bg-2019-462
Preprint. Discussion started: 7 January 2020

et al., 2014; Haley et al., 2005; Sholkovitz and Shen, 1995). However, this hypothesis does not hold at station #21 where $CaCO_3$ concentration is high while the PCe anomaly is positive (Fig. S4 in supplementary). A surface photoreduction could explain the surface weak anomalies by reducing Ce(IV) in Ce(III) that can be desorbed from particles. The MnO_2 depletion in the surface waters of NADR region would support this hypothesis, although this MnO_2 depletion reaches 500 m (ie below the euphotic layer, Fig S6A in supplementary). In the NAST region, a MnO_2 surface minimum occurs too, but does not correspond to a PCe/Ce* minimum.

4.4 The influence of biological activity on the REE distributions

4.2 The influence of biological activity on the REE distributions

The surface of open-sea stations (all of them except #1 and #53) are characterized by a higher lithogenic proportion for LREEs than for HREEs, meaning that the expected relative enrichment of the authigenic phase in LREE -due to their lower solubility- is not observed (see the vertical profiles reported in Fig. 5). Thus, an uncommon enrichment of the authigenic material in HREEs is observed in these samples, also shown in the total PREE patterns (Fig. 5 and Fig. S4 in supplementary). Indeed, these patterns display a negative Ce anomaly on the first hundred meters and enrichment in HREEs characterized by high PYbN/PNdN ratios (>1, Fig. 4) that can reach 1000 m. Such kind of pattern is classically observed for dissolved REEs, more rarely for PREEs. Suspended PREEs displaying such “dissolved–type” pattern suggest that they have been likely formed through absorption than adsorption processes, the latter leading to fractionation between the REEs, which is not the case during the uptake of REEs in the carbonate planktonic shells (Palmer and Elderfield, 1986). The negative PCe anomaly (Fig. 7) suggests recently formed particles on which Ce oxidation leading to positive PCe anomaly have not occurred yet. All these stations are subject to a strong primary production (Fonseca-Batista et al., 2019), so the preferential transfer of HREEs from the dissolved phase to the authigenic particulate one likely occurs when the biological stripping is active. However, this transfer is more important in the ARCT region than in the NADR region, leading to stronger HREE enrichments, while the highest bloom activity was observed in the NADR region with a maximum at station #26. The high prevalence of coccolithophorids characterizing this bloom (Lemaitre et al., 2018) could explain the relatively low HREE enrichment, except at station #26. In the NADR region, the patterns flatten with depth to present a quasi-lithogenic signature under 60 m, suggesting that particles with a strong organic signature have not reach this depth yet. In the ARCT region, the bloom was dominated by diatoms, still active at station #51 and declining at the others (Fonseca-Batista et al., 2019; Lemaitre et al., 2018).This declining bloom leads to a strong export, but high remineralization rates decrease the biological signature proportion in favor of the lithogenic one at depth (Fig. 5). Even if the characterization of the authigenic phase leans on 232Th and the assumption that REEs and 232Th behave similarly from the original lithogenic source, it is thus very likely that biological uptake appears to have a strong effect on the total REE patterns observed.

A relationship between HREEs and biogenic matter, mostly BSi, have been suggested by Akagi (2013) following thermodynamic calculations. According to this work, 10% to 20% of REEs are forming a REE(H3SiO4)2+ complex with silicic acid, this proportion being more important as the atomic number is low and with depth. Complexation of REE with

https://doi.org/10.5194/bg-2019-462
Preprint. Discussion started: 7 January 2020

385 silicates was further confirmed by Patten and Byrne (2017), although these authors estimated lower complexation constant, thus a less important fraction of REEs complexed by silica. In addition, significant correlations were observed between dissolved Si and dissolved HREE by Bertram and Elderfield (1992; western Indian Ocean), Akagi et al. (2011, North Pacific Ocean); Stichel et al. (2012) and Garcia-Solsona et al. (2014), both in the Atlantic sector of Southern Ocean), Grenier et al. (2018; Kerguelen Islands) and Pham et al. (2019; Solomon Sea). Contrastingly in other areas, the correlation between $SiOH_4$
390 and REEs present a curvature or is absent (Patten and Byrne, 2017, their Fig. 7; Zheng et al., 2016, their Fig. 11). Even if the causes of such relationships are not clear, the PYbN/PNdN ratio in the authigenic phase is the highest between the surface and 50 m in the Irminger Sea and the Labrador Sea, where BSi concentrations are also the highest (Sarthou et al., 2018), reflecting a bloom dominated by diatom species (Fig. S5A and B in supplementary material). Although the correlation between BSi and PHREEs stays weak (from R^2=0.06 for Ho to R^2=0.4 for Lu), this correlation coefficient rises with the atomic mass number
395 (Fig. S5C), showing that BSi has a significant influence on authigenic PREE distributions from Tb to Lu that does not appear for lighter REEs. These correlations may show that in some areas the HREE distributions are linked to the biogeochemistry of silicate, and not only to a conservative mixing as shown by Zheng et al. (2016) and de Baar et al. (2018). This relationship would depends on the abundance and the nature of particles (the occurrence of diatoms), and on the speciation of REEs in the dissolved phase as shown by de Baar et al. (2018). Akagi, (2013) and Akagi et al. (2011) proposed an incorporation of the
400 silica-REEs complexes during the frustules construction, but the mechanism under this enrichment during diatom blooms remains to be clarified. Linking it to usual complexation and adsorption processes is not straightforward since this would imply a sharp break between LREE and HREE affinities with BSi, which has still to be demonstrated. In addition, an effective relationship between BSi and PHREE can be blurred by other scavenging processes implying particulate Mn and Fe (hydr)oxides, also known to influence the slope between LREE and HREE.

405 **4.5 The PAAS-normalized particulate Ho/Y ratio: a proxy of processes independent of the ionic radius**

Yttrium (Y) and the lanthanide holmium (Ho) are characterized by about the same ionic radius and identical charge, making them "geochemical twins" (Bau, 1999). The PAAS-normalized particulate ratio (PHoN/PYN) highlights differences in their distributions, and therefore allows identifying radius-independent fractionation processes affecting YREE in seawater. We choose to normalize PHo/PY measured in our particulate samples to the PAAS ratio to reveal any relative loss or enrichment
410 compared to continental material (Fig. 8). Due to differences of electron configuration, Ho is more prone to establish ionic bounds, and then to be preferentially scavenged by adsorption onto (hydr)oxides as $FeOH_3$ and MnO_2. In comparison, Y is preferentially scavenged when covalent bounds are established (Censi et al., 2007; Bau, 1999; Bau et al., 1995). Along the GEOVIDE section, PHoN/PYN ratio varies between 0.4 and 1.5, with most of the values less than 1 (i.e. depleted compared to PAAS), which does not support the expected preferential scavenging of Ho. Moreover, PHoN/PYN relationship with $FeOH_3$
415 and MnO_2 doesn't fit to any pattern (Fig. 9). PHoN/PYN is higher when $[Fe(OH)_3]$> 10-2 µg.L-1, while there is no evidence of a higher HoN/YN ratio when MnO_2 content increases. However, while there is a pronounced east-west gradient in the

https://doi.org/10.5194/bg-2019-462
Preprint. Discussion started: 7 January 2020

Fe(OH)3 distribution, the PHoN/PYN ratio (Fig. S6 in supplementary) is low (<0.6) in Labrador Sea surface waters (station #69), the Irminger Sea (stations #44 and #51) and from the surface to 750 m in the NADR region (stations #21, #26 and #32). These locations are depleted in both MnO2 and Fe(OH)3 (Fig. S6 in supplementary), leading to a weak adsorption of Ho. All along the section, low ratios are observed at the surface and until 800 m in the areas of marked biological productivity (stations #26, #32, #69), although they are directly linked to primary production intensity. This suggests a preferential scavenging of Y during the formation of biogenic matter, as reported by Censi et al. (2007), and not through simple adsorption which would support preferential scavenging of Ho. In the NADR region, at depths between 200 m and 600 m that are characterized by strong and positive PCe anomaly and a persistent PHREE enrichment, a PHo depletion is observed at stations #26 and #21. The low remineralization rates observed in this area could make persistent the PY enrichment formed at the surface, when the positive PCe anomaly suggests that a dynamic scavenging occurs. The difference between those two elements can be explained by a preferential scavenging of LREE compared to HREE during adsorption processes. The PHo enrichment at station #32 between 350 m and 600 m goes with the most important Ce positive anomaly, indicating intensive exchanges by adsorption with the dissolved phase, and then a stronger scavenging of REEs.

In the ARCT region, slightly lower ratios are observed at station #69 than for others, and this station is characterized by a lower primary production and the higher remineralization rates along the section (Lemaitre et al., 2018). Ho, more adsorbed than Y is then more prone to be released, leading to a lower signal due to the Y enrichment of the covalent part of the particles, less easily remineralized. The higher ratios at other ARCT stations indicate scavenging by particles, although the Ce anomaly is lower than in the NADR region.

Thus, our results show that high PHoN/PYN ratio not only reflects sorption processes driven by the occurrence of Fe(OH)3 and to a lesser extent MnO2 but all processes favoring outer-sphere complex formation, which would promote Ho and other REEs scavenging compared to Y. The relationship with particle production, particle residence time and remineralization rates is not clear indicating the influence of other parameters not identified yet.

References

Akagi, T.: Rare earth element (REE)–silicic acid complexes in seawater to explain the incorporation of REEs in opal and the "leftover" REEs in surface water: New interpretation of dissolved REE distribution profiles, Geochimica et Cosmochimica Acta, 113, 174–192, doi:10.1016/j.gca.2013.03.014, 2013.

Aries, S., Valladon, M., Polvé, M. and Dupré, B.: A Routine Method for Oxide and Hydroxide Interference Corrections in ICP-MS Chemical Analysis of Environmental and Geological Samples, Geostandards and Geoanalytical Research, 24(1), 19–31, doi:10.1111/j.1751-908X.2000.tb00583.x, 2000.

Bau, M.: Scavenging of dissolved yttrium and rare earths by precipitating iron oxyhydroxide: Experimental evidence for Ce oxidation, Y-Ho fractionation, and lanthanide tetrad effect, Geochim. Cosmochim. Ac., 63(1), 67–77, 1999.

https://doi.org/10.5194/bg-2019-462
Preprint. Discussion started: 7 January 2020

Bau, M. and Koschinsky, A.: Oxidative scavenging of cerium on hydrous Fe oxide: Evidence from the distribution of rare earth elements and yttrium between Fe oxides and Mn oxides in hydrogenetic ferromanganese crusts, Geochem. J., 43(1), 37–47, doi:10.2343/geochemj.1.0005, 2009.

Bau, M., Koschinsky, A., Dulski, P. and Hein, J. R.: Comparison of the partitioning behaviours of yttrium, rare earth elements, and titanium between hydrogenetic marine ferromanganese crusts and seawater, Geochim. Cosmochim. Ac., 60(10), 1709–1725, 1996.

Bayon, G., German, C. R., Burton, K. W., Nesbitt, R. W. and Rogers, N.: Sedimentary Fe–Mn oxyhydroxides as paleoceanographic archives and the role of aeolian flux in regulating oceanic dissolved REE, Earth and Planetary Science Letters, 224(3–4), 477–492, doi:10.1016/j.epsl.2004.05.033, 2004.

Bertram, C.J. and Elderfield, H.: The geochemical balance of the rare earth elements and neodymium isotopes in the oceans, Geochim. Cosmochim. Ac., 57, 1957–1986, 1992.

Bolhar, R., Kamber, B. S., Moorbath, S., Fedo, C. M. and Whitehouse, M. J.: Characterisation of early Archaean chemical sediments by trace element signatures, Earth and Planetary Science Letters, 222(1), 43–60, doi:10.1016/j.epsl.2004.02.016, 2004.

Byrne, R. H. and Kim, K.-H.: Rare earth element scavenging in seawater, Geochimica et Cosmochimica Acta, 54(10), 2645–2656, doi:10.1016/0016-7037(90)90002-3, 1990.

Cacchione, D. A.: The Shaping of Continental Slopes by Internal Tides, Science, 296(5568), 724–727, doi:10.1126/science.1069803, 2002.

Daniault, N., Mercier, H., Lherminier, P., Sarafanov, A., Falina, A., Zunino, P., Pérez, F. F., Ríos, A. F., Ferron, B., Huck, T., Thierry, V. and Gladyshev, S.: The northern North Atlantic Ocean mean circulation in the early 21st century, Progress in Oceanography, 146, 142–158, doi:10.1016/j.pocean.2016.06.007, 2016.

Elderfield, H.: The oceanic chemistry of the rare-earth elements, Philosophical Transactions of the Royal Society of London, A(325), 105–126, 1988.

van de Flierdt, T., Pahnke, K., Amakawa, H., Andersson, P., Basak, C., Coles, B., Colin, C., Crocket, K., Frank, M., Frank, N., Goldstein, S. L., Goswami, V., Haley, B. A., Hathorne, E. C., Hemming, S. R., Henderson, G. M., Jeandel, C., Jones, K., Kreissig, K., Lacan, F., Lambelet, M., Martin, E. E., Newkirk, D. R., Obata, H., Pena, L., Piotrowski, A. M., Pradoux, C., Scher, H. D., Schöberg, H., Singh, S. K., Stichel, T., Tazoe, H., Vance, D. and Yang, J.: GEOTRACES intercalibration of neodymium isotopes and rare earth element concentrations in seawater and suspended particles. Part 1: reproducibility of results for the international intercomparison: Intercalibration of Seawater Nd Isotopes, Limnol. Oceanogr. Methods, 10(4), 234–251, doi:10.4319/lom.2012.10.234, 2012.

Fonseca-Batista, D., Li, X., Riou, V., Michotey, V., Deman, F., Fripiat, F., Guasco, S., Brion, N., Lemaitre, N., Tonnard, M., Gallinari, M., Planquette, H., Planchon, F., Sarthou, G., Elskens, M., LaRoche, J., Chou, L. and Dehairs, F.: Evidence of high N₂ fixation rates in the temperate northeast Atlantic, Biogeosciences, 16(5), 999–1017, doi:10.5194/bg-16-999-2019, 2019.

García-Ibáñez, M. I., Pardo, P. C., Carracedo, L. I., Mercier, H., Lherminier, P., Ríos, A. F. and Pérez, F. F.: Structure, transports and transformations of the water masses in the Atlantic Subpolar Gyre, Progress in Oceanography, 135, 18–36, doi:10.1016/j.pocean.2015.03.009, 2015.

García-Ibáñez, M. I., Pérez, F. F., Lherminier, P., Zunino, P., Mercier, H. and Tréguer, P.: Water mass distributions and transports for the 2014 GEOVIDE cruise in the North Atlantic, Biogeosciences, 15(7), 2075–2090, doi:10.5194/bg-15-2075-2018, 2018.

Garcia-Solsona, Esther, Jeandel, Catherine, Labatut, Marie, Lacan, François, Vance, Derek, Chavagnac, Valérie and Pradoux, Catherine: Rare earth elements and Nd isotopes tracing water mass mixing and particle-seawater interactions in the SE Atlantic, Geochim. Cosmochim. Ac., 125, 351–372, 2014.

Gehlen, M., Bopp, L., Emprin, N., Aumont, O., Heinze, C. and Ragueneau, O.: Reconciling surface ocean productivity, export fluxes and sediment composition in a global biogeochemical ocean model, , 17, 2006.

Gourain, A., Planquette, H., Cheize, M., Lemaitre, N., Menzel Barraqueta, J.-L., Shelley, R., Lherminier, P. and Sarthou, G.: Inputs and processes affecting the distribution of particulate iron in the North Atlantic along the GEOVIDE (GEOTRACES GA01) section, Biogeosciences, 16(7), 1563–1582, doi:10.5194/bg-16-1563-2019, 2019.

Grenier, M.: Differentiating Lithogenic Supplies, Water Mass Transport, and Biological Processes On and Off the Kerguelen Plateau Using Rare Earth Element Concentrations and Neodymium Isotopic Compositions, Frontiers in Marine Science, 5, 30, 2018.

Guichard, F., Church, T. M., Treuil, M. and Jaffrezic, H.: Rare earths in barites: distribution and effects on aqueous partitioning, Geochimica et Cosmochimica Acta, 43(7), 983–997, doi:10.1016/0016-7037(79)90088-7, 1979.

Haley, B. A., Klinkhammer, G. P. and Mix, A. C.: Revisiting the rare earth elements in foraminiferal tests, Earth and Planetary Science Letters, 239(1–2), 79–97, doi:10.1016/j.epsl.2005.08.014, 2005.

Hayes, C. T., Anderson, R. F., Fleisher, M. Q., Vivancos, S. M., Lam, P. J., Ohnemus, D. C., Huang, K.-F., Robinson, L. F., Lu, Y., Cheng, H., Edwards, R. L. and Moran, S. B.: Intensity of Th and Pa scavenging partitioned by particle chemistry in the North Atlantic Ocean, Marine Chemistry, 170, 49–60, doi:10.1016/j.marchem.2015.01.006, 2015.

Jeandel, C., Bishop, J. K. and Zindler, A.: Exchange of neodymium and its isotopes between seawater and small and large particles in the Sargasso Sea, Geochimica et Cosmochimica Acta, 59(3), 535–547, doi:10.1016/0016-7037(94)00367-U, 1995.

de Jong, M. F. and de Steur, L.: Strong winter cooling over the Irminger Sea in winter 2014-2015, exceptional deep convection, and the emergence of anomalously low SST: IRMINGER SEA COOLING AND CONVECTION, Geophys. Res. Lett., 43(13), 7106–7113, doi:10.1002/2016GL069596, 2016.

Khatiwala, S., Tanhua, T., Mikaloff Fletcher, S., Gerber, M., Doney, S. C., Graven, H. D., Gruber, N., McKinley, G. A., Murata, A., Ríos, A. F. and Sabine, C. L.: Global ocean storage of anthropogenic carbon, Biogeosciences, 10(4), 2169–2191, doi:10.5194/bg-10-2169-2013, 2013.

Kuss, J., Garbe-Schönberg, C.-D. and Kremling, K.: Rare earth elements in suspended particulate material of North Atlantic surface waters, Geochimica et Cosmochimica Acta, 65(2), 187–199, doi:10.1016/S0016-7037(00)00518-4, 2001.

Lacan, F. and Jeandel, C.: Acquisition of the neodymium isotopic composition of the North Atlantic Deep Water: NEODYMIUM ISOTOPIC COMPOSITION, Geochemistry, Geophysics, Geosystems, 6(12), n/a-n/a, doi:10.1029/2005GC000956, 2005.

Lam, P. J., Twining, B. S., Jeandel, C., Roychoudhury, A., Resing, J. A., Santschi, P. H. and Anderson, R. F.: Methods for analyzing the concentration and speciation of major and trace elements in marine particles, Progress in Oceanography, 133, 32–42, doi:10.1016/j.pocean.2015.01.005, 2015.

Lemaitre, N., Planquette, H., Planchon, F., Sarthou, G., Jacquet, S., García-Ibáñez, M. I., Gourain, A., Cheize, M., Monin, L., André, L., Laha, P., Terryn, H. and Dehairs, F.: Particulate barium tracing of significant mesopelagic carbon remineralisation in the North Atlantic, Biogeosciences, 15(8), 2289–2307, doi:10.5194/bg-15-2289-2018, 2018.

Lerner, P., Marchal, O., Lam, P. J. and Solow, A.: Effects of particle composition on thorium scavenging in the North Atlantic, Geochimica et Cosmochimica Acta, 233, 115–134, doi:10.1016/j.gca.2018.04.035, 2018.

Lherminier, P. and Sarthou, G.: The 2014 Greenland-Portugal GEOVIDE CTDO2 hydrographic and SADCP data (GO-SHIP A25 and GEOTRACES GA01), SEANOE, doi:https://doi.org/10.17882/52153, 2017.

Longhurst, A.: Seasonal cycles of pelagic production and consumption, Progress in Oceanography, 36(2), 77–167, doi:10.1016/0079-6611(95)00015-1, 1995.

McCave, I. . and Hall, I. .: Turbidity of waters over the Northwest Iberian continental margin, Progress in Oceanography, 52(2–4), 299–313, doi:10.1016/S0079-6611(02)00012-5, 2002.

Menzel Barraqueta, J.-L., Schlosser, C., Planquette, H., Gourain, A., Cheize, M., Boutorh, J., Shelley, R., Contreira Pereira, L., Gledhill, M., Hopwood, M. J., Lacan, F., Lherminier, P., Sarthou, G. and Achterberg, E. P.: Aluminium in the North Atlantic Ocean and the Labrador Sea (GEOTRACES GA01 section): roles of continental inputs and biogenic particle removal, Biogeosciences, 15(16), 5271–5286, doi:10.5194/bg-15-5271-2018, 2018.

Moffett, J. W.: Microbially mediated cerium oxidation in sea water, Nature, 345(6274), 421–423, doi:10.1038/345421a0, 1990.

Moffett, J. W.: The relationship between cerium and manganese oxidation in the marine environment, Limnol. Oceanogr., 39(6), 1309–1318, doi:10.4319/lo.1994.39.6.1309, 1994.

Palmer, M. R.: Rare earth elements in foraminifera tests, Earth and Planetary Science Letters, 73, 285–298, 1985.

Patey, M. D., Achterberg, E. P., Rijkenberg, M. J. and Pearce, R.: Aerosol time-series measurements over the tropical Northeast Atlantic Ocean: Dust sources, elemental composition and mineralogy, Marine Chemistry, 174, 103–119, doi:10.1016/j.marchem.2015.06.004, 2015.

Pham, V. Q., Grenier, M., Cravatte, S., Michael, S., Jacquet, S., Belhadj, M., Nachez, Y., Germineaud, C. and Jeandel, C.: Dissolved rare earth elements distribution in the Solomon Sea, Chemical Geology, 524, 11–36, doi:10.1016/j.chemgeo.2019.05.012, 2019.

Phoebe J. Lam, Jong-Mi Lee, Maija I. Heller, Sanjin Mehic, Yang Xiang and Nicholas R. Bates: Size-fractionated distributions of suspended particle concentration and major phase composition from the U.S. GEOTRACES Eastern Pacific Zonal Transect (GP16), Mar. Chem., doi:http://dx.doi.org/10.1016/j.marchem.2017.08.013, 2017.

Planquette, H. and Sherrell, R. M.: Sampling for particulate trace element determination using water sampling bottles: methodology and comparison to in situ pumps, Limnology and Oceanography: Methods, 10(5), 367–388, doi:10.4319/lom.2012.10.367, 2012.

R, S.: Ocean Data View, [online] Available from: http://odv.awi.de, 2016.

Rea, D. K.: The paleoclimatic record provided by eolian deposition in the deep sea: The geologic history of wind, Rev. Geophys., 32(2), 159, doi:10.1029/93RG03257, 1994.

Reygondeau, G., Guidi, L., Beaugrand, G., Henson, S. A., Koubbi, P., MacKenzie, B. R., Sutton, T. T., Fioroni, M. and Maury, O.: Global biogeochemical provinces of the mesopelagic zone, Journal of Biogeography, 45(2), 500–514, doi:10.1111/jbi.13149, 2018.

Rudnick, R. L. and Gao, S.: Composition of the Continental Crust, in Treatise on Geochemistry, pp. 1–51, Elsevier., 2014.

Sanders, R., Henson, S. A., Koski, M., De La Rocha, C. L., Painter, S. C., Poulton, A. J., Riley, J., Salihoglu, B., Visser, A., Yool, A., Bellerby, R. and Martin, A. P.: The Biological Carbon Pump in the North Atlantic, Progress in Oceanography, 129, 200–218, doi:10.1016/j.pocean.2014.05.005, 2014.

Schijf, J., Christenson, E. A. and Byrne, R. H.: YREE scavenging in seawater: A new look at an old model, Marine Chemistry, 177, 460–471, doi:10.1016/j.marchem.2015.06.010, 2015.

Shelley, R. U., Roca-Martí, M., Castrillejo, M., Sanial, V., Masqué, P., Landing, W. M., Beek, P. van, Planquette, H. and Sarthou, G.: Quantification of trace element atmospheric deposition fluxes to the Atlantic Ocean (>40°N; GEOVIDE, GEOTRACES GA01) during spring 2014, Deep Sea Research Part I: Oceanographic Research Papers, 119, 34–49, doi:https://doi.org/10.1016/j.dsr.2016.11.010, 2017.

Sholkovitz, E. and Shen, G. T.: The incorporation of rare earth elements in modern coral, Geochimica et Cosmochimica Acta, 59(13), 2749–2756, doi:10.1016/0016-7037(95)00170-5, 1995.

Sholkovitz, E. R., Landing, W. M. and Lewis, B. L.: Ocean particle chemistry: The fractionation of rare earth elements between suspended particles and seawater, Geochimica et Cosmochimica Acta, 58(6), 1567–1579, doi:10.1016/0016-7037(94)90559-2, 1994.

Stemmann, L., Gorsky, G., Marty, J.-C., Picheral, M. and Miquel, J.-C.: Four-year study of large-particle vertical distribution (0–1000m) in the NW Mediterranean in relation to hydrology, phytoplankton, and vertical flux, Deep Sea Research Part II: Topical Studies in Oceanography, 49(11), 2143–2162, doi:10.1016/S0967-0645(02)00032-2, 2002.

Tachikawa, K., Handel, C. and Dupré, B.: Distribution of rare earth elements and neodymium isotopes in settling particulate material of the tropical Atlantic Ocean (EUMELI site), Deep Sea Research Part I: Oceanographic Research Papers, 44(11), 1769–1792, doi:10.1016/S0967-0637(97)00057-5, 1997.

Tachikawa, K., Jeandel, C., Vangriesheim, A. and Dupré, B.: Distribution of rare earth elements and neodymium isotopes in suspended particles of the tropical Atlantic Ocean (EUMELI site), Deep Sea Research Part I: Oceanographic Research Papers, 46(5), 733–755, doi:10.1016/S0967-0637(98)00089-2, 1999.

https://doi.org/10.5194/bg-2019-462
Preprint. Discussion started: 7 January 2020

Tonnard, M., Planquette, H., Bowie, A. R., van der Merwe, P., Gallinari, M., Desprez de Gésincourt, F., Germain, Y., Gourain, A., Benetti, M., Reverdin, G., Tréguer, P., Boutorh, J., Cheize, M., Menzel Barraqueta, J.-L., Pereira-Contreira, L., Shelley, R., Lherminier, P. and Sarthou, G.: Dissolved iron in the North Atlantic Ocean and Labrador Sea along the GEOVIDE section (GEOTRACES section GA01), Biogeosciences Discussions, 1–53, doi:10.5194/bg-2018-147, 2018.

Van Beueskom, J. E. E., Van Bennekom, A. J., Tréguer, P. and Morvan, J.: Aluminium and silicic acid in water and sediments of the Enderby and Crozet Basins, Deep Sea Research Part II: Topical Studies in Oceanography, 44(5), 987–1003, doi:10.1016/S0967-0645(96)00105-1, 1997.

Yeghicheyan, D., Bossy, C., Bouhnik Le Coz, M., Douchet, C., Granier, G., Heimburger, A., Lacan, F., Lanzanova, A., Rousseau, T. C. C., Seidel, J.-L., Tharaud, M., Candaudap, F., Chmeleff, J., Cloquet, C., Delpoux, S., Labatut, M., Losno, R., Pradoux, C., Sivry, Y. and Sonke, J. E.: A Compilation of Silicon, Rare Earth Element and Twenty-One other Trace Element Concentrations in the Natural River Water Reference Material SLRS-5 (NRC-CNRC), Geostandards and Geoanalytical Research, 37(4), 449–467, doi:10.1111/j.1751-908X.2013.00232.x, 2013.

Zheng, X.-Y., Plancherel, Y., Saito, M. A., Scott, P. M. and Henderson, G. M.: Rare earth elements (REEs) in the tropical South Atlantic and quantitative deconvolution of their non-conservative behavior, Geochimica et Cosmochimica Acta, 177, 217–237, doi:10.1016/j.gca.2016.01.018, 2016.

Zunino, P., Lherminier, P., Mercier, H., Daniault, N., García-Ibáñez, M. I. and Pérez, F. F.: The GEOVIDE cruise in May–June 2014 reveals an intense Meridional Overturning Circulation over a cold and fresh subpolar North Atlantic, Biogeosciences, 14(23), 5323–5342, doi:10.5194/bg-14-5323-2017, 2017.

https://doi.org/10.5194/bg-2019-462
Preprint. Discussion started: 7 January 2020


Biogeosciences Discussions Open Access EGU

Table 1: List of region, water masse and current abbreviations.

Regions	
SPNA	Subpolar North Atlantic
NAST	North Atlantic Subtropical
NADR	North Atlantic drift
ARCT	Arctic
Water masses	
ENACW	East North Atlantic Central Water
MW	Mediterranean Water
SPMW	Subpolar Mode Water
IrSPMW	Irminger Subpolar Mode Water
LSW	Irminger Subpolar Mode Water
Currents	
NAC	North Atlantic Current
ERRC	East Reykjanes Ridge Current
IC	Irminger Current
EGIC	East Greenland Irminger Current
EGCC	East Greenland Coastal Current

620 **Table 2: Particulate REE, Y, Ba and ^{232}Th concentrations with the corresponding 2σ error.**

https://doi.org/10.5194/bg-2019-462
Preprint. Discussion started: 7 January 2020

Biogeosciences
Discussions
Open Access
EGU

Station	Longitude	Latitude	Depth [m]	La	2σ	Ce	2σ	Pr	2σ	Nd	2σ	Sm	2σ	Eu	2σ	Gd	2σ	Tb	2σ	Dy	2σ	Ho	2σ	Er	2σ	Tm	2σ	Yb	2σ	Lu	2σ	Y	2σ	Ba	2σ	Th	2σ
1	-10.0359	40.333	20	962	234	1997	476	216	54	757	182	159	41	32	8	124	31	18	5	107	26	20	5	51	14	8	2	49	12	5	1	1321	321	168667	43630	1031	45
1	-10.0359	40.333	40	1730	377	2904	635	367	85	1377	326	333	77	60	13	238	53	35	8	192	44	36	8	97	25	13	3	82	18	8	2	2908	631	269439	59703	150	36
1	-10.0359	40.333	60	596	133	1101	245	61	15	218	51	47	12	11	3	44	10	7	2	41	9	8	2	23	6	4	1	21	5	2	0	382	90	246857	55972	51	12
1	-10.0359	40.333	79	1014	214	1497	317	155	34	510	111	112	30	22	5	95	21	31	7	71	16	14	3	39	10	6	1	36	8	4	1	948	206	406435	85960	113	24
1	-10.0359	40.333	98	1552	365	2848	657	289	77	1061	252	222	63	44	10	153	40	20	5	125	29	23	5	68	19	9	2	57	14	7	2	1443	351	501392	127194	180	43
1	-10.0359	40.333	119	1248	320	2649	677	273	78	955	267	230	68	37	9	147	37	20	6	116	30	22	5	58	16	8	2	56	14	7	2	1321	345	384719	105833	187	49
1	-10.0359	40.333	139	1303	317	3179	773	260	64	963	234	214	54	36	9	147	35	57	15	111	27	20	5	58	15	7	2	49	12	6	1	994	246	346096	88913	203	49
1	-10.0359	40.333	160	1466	384	3938	1015	317	91	1123	299	228	73	46	12	172	48	22	6	126	34	23	6	62	17	8	3	57	15	7	2	1644	441	323704	93522	221	58
1	-10.0359	40.333	200	2591	579	6041	1335	578	131	2090	470	362	86	77	17	282	66	38	9	213	48	38	8	104	24	14	3	93	21	12	3	1848	419	400111	90744	475	109
1	-10.0359	40.333	249	3458	935	7935	2045	769	213	2815	724	535	158	105	27	392	100	57	16	286	74	50	13	133	37	19	6	124	32	17	4	2464	658	618995	173326	573	151
1	-10.0359	40.333	299	3735	970	8831	2298	904	259	3001	850	443	130	109	28	401	103	53	15	301	77	53	14	133	35	20	6	130	33	17	4	2558	672	428470	120773	684	173
1	-10.0359	40.333	309	2553	654	5692	1421	602	167	2139	644	626	161	77	19	308	76	41	11	234	68	43	11	118	33	17	5	107	27	14	3	2218	569	326470	89328	433	105
1	-10.0359	40.333	499	2821	726	6219	1590	654	196	2426	698	483	145	90	24	338	107	47	13	253	79	46	12	122	36	18	5	111	29	14	4	2219	582	397429	104586	500	129
1	-10.0359	40.333	597	3392	817	7103	1706	733	179	2593	629	496	131	97	24	330	88	81	20	259	63	47	11	127	32	18	5	113	27	15	4	2352	574	589423	143050	484	118
1	-10.0359	40.333	702	5732	1400	9612	2346	1228	301	4505	1113	826	217	184	45	656	177	103	26	610	148	121	29	333	85	45	11	280	68	39	9	7731	1893	244048	59668	719	176
1	-10.0359	40.333	800	2554	610	5303	1264	558	136	1979	477	366	95	70	17	239	63	36	9	200	48	37	9	103	26	14	3	91	22	12	3	1989	478	231312	55034	417	102
1	-10.0359	40.333	1000	2558	601	5145	1201	557	132	1994	471	378	98	90	21	276	65	41	11	222	54	41	10	112	27	16	4	98	23	13	3	3594	843	237640	55706	374	88
1	-10.0359	40.333	1505	3644	961	7402	1916	844	240	2849	744	497	134	71	18	286	78	41	12	221	57	40	10	108	32	15	4	94	24	12	3	2217	588	210230	57446	361	91
13	-13.8877	41.383	20	1381	462	3330	1102	290	101	1113	365	422	137	61	21	182	59	26	9	138	45	26	8	80	29	10	4	65	21	8	3	1380	460	385242	131035	176	57
13	-13.8877	41.383	40	1219	380	3035	324	187	58	785	246	202	65	57	18	254	80	50	16	403	125	106	33	388	122	69	21	496	153	82	25	6313	1986	217104	67714	69	21
13	-13.8877	41.383	60	999	313	893	279	125	40	414	131	91	32	23	8	99	31	18	6	109	35	26	8	90	28	15	5	108	33	16	5	1476	466	179211	56139	71	22
13	-13.8877	41.383	78	918	285	1467	456	135	42	500	157	101	34	23	7	100	31	21	7	104	33	24	7	80	26	13	4	98	30	15	5	2449	767	247745	77277	80	25
13	-13.8877	41.383	100	612	187	1004	308	117	36	429	133	88	31	20	6	91	31	13	4	81	25	17	5	55	17	8	3	62	19	9	3	992	309	280866	85623	74	22
13	-13.8877	41.383	120	853	262	1375	423	122	38	460	142	82	28	20	7	88	27	12	4	79	26	16	5	49	16	8	3	53	17	8	2	869	285	302221	93035	71	22
13	-13.8877	41.383	140	775	237	1356	416	147	46	541	166	115	38	25	8	98	31	14	5	82	25	17	5	50	16	7	2	52	16	7	2	1039	324	358546	110038	95	29
13	-13.8877	41.383	160	1258	395	3917	1226	225	72	823	259	161	52	35	11	166	58	25	8	169	53	36	11	111	35	17	6	115	36	17	5	1904	601	455716	142611	345	107
13	-13.8877	41.383	200	741	255	1075	359	142	48	557	188	117	45	33	12	114	38	15	5	95	34	18	6	54	20	8	3	52	17	7	3	1029	362	411899	145918	76	26
13	-13.8877	41.383	250	1418	482	2443	822	244	88	1029	357	214	77	67	23	178	60	52	19	145	51	30	10	85	30	12	4	87	29	12	4	1691	583	532827	184463	185	61
13	-13.8877	41.383	300	1833	592	2871	924	279	91	893	288	102	35	52	17	110	35	18	6	113	38	24	8	78	27	10	3	70	22	10	3	1301	425	575153	191525	77	25
13	-13.8877	41.383	400	979	299	1610	494	190	59	731	224	139	48	30	10	128	40	18	6	102	32	19	6	50	16	7	3	49	15	6	2	955	298	941793	286891	98	30
13	-13.8877	41.383	500	964	323	2325	769	202	71	777	255	295	96	43	14	127	41	18	6	96	31	18	6	56	20	7	3	45	15	6	2	963	321	269007	91499	123	40
13	-13.8877	41.383	600	774	251	2113	675	160	56	900	280	126	47	25	8	107	34	14	5	88	29	17	5	48	17	7	3	46	15	5	2	862	283	302553	103074	144	45
13	-13.8877	41.383	700	806	253	2070	647	165	52	597	188	119	39	26	8	113	37	16	5	90	29	18	6	50	16	7	2	46	14	6	2	1057	337	311054	97659	107	34
13	-13.8877	41.383	800	917	280	2192	669	201	63	741	227	145	47	30	9	125	39	17	6	98	31	19	6	52	17	8	2	49	15	6	2	941	292	264766	80417	135	41
13	-13.8877	41.383	1000	977	327	2356	780	205	72	765	251	148	52	43	14	129	42	18	6	97	34	18	6	57	19	7	3	46	15	6	2	976	325	272625	92729	124	40
13	-13.8877	41.383	1501	1026	353	2379	811	209	72	785	268	149	57	32	11	142	51	22	8	94	32	18	6	47	18	7	3	46	16	6	2	1715	597	192673	69010	154	52
21	-19.6724	46.544	10	978	244	1188	290	153	37	555	137	108	30	30	7	113	28	20	5	123	31	28	7	94	23	15	4	115	29	19	5	2165	535	228160	56824	76	19
21	-19.6724	46.544	20	3837	999	7279	1896	260	68	862	224	167	51	51	14	214	63	43	12	175	47	37	9	112	31	18	5	130	34	21	5	3112	831	609765	163707	150	38
21	-19.6724	46.544	40	756	189	812	199	89	22	325	82	68	18	17	4	69	18	n.d.	n.d.	65	17	14	3	42	11	6	2	47	12	7	2	1127	287	333496	83648	60	15
21	-19.6724	46.544	60	962	241	1433	358	195	51	764	189	147	43	26	7	148	38	13	4	147	39	20	5	67	20	11	3	71	18	10	2	1459	365	213886	54792	74	18
21	-19.6724	46.544	76	988	257	1824	471	171	46	652	174	122	32	32	8	118	31	16	5	97	27	20	5	57	16	8	2	58	16	7	2	1102	298	551682	147043	88	23
21	-19.6724	46.544	100	9587	2397	15591	3806	917	230	2870	720	129	33	28	7	120	30	18	6	93	24	18	5	51	13	7	2	46	11	6	2	948	237	477465	119403	76	19
21	-19.6724	46.544	120	787	191	1312	318	162	41	681	165	125	37	32	8	110	26	16	4	83	21	16	4	44	12	6	1	40	9	5	1	816	200	495584	121374	58	14
21	-19.6724	46.544	140	1050	256	2456	605	195	49	745	191	114	32	34	9	123	30	17	5	90	24	17	4	45	12	7	2	42	11	6	1	950	235	515979	130504	96	24
21	-19.6724	46.544	160	404	98	774	187	88	23	327	80	77	19	28	7	69	16	10	3	57	15	11	3	31	9	4	1	30	7	3	1	662	167	352326	91426	51	12
21	-19.6724	46.544	200	634	160	1071	266	133	34	522	133	111	29	28	7	99	25	14	4	78	21	15	4	41	11	6	2	36	9	5	1	784	200	354634	91804	53	13
21	-19.6724	46.544	300	751	182	2121	509	146	37	567	138	113	30	33	8	110	27	16	4	90	24	17	4	50	14	7	2	43	11	6	1	1016	246	517097	129908	65	16
21	-19.6724	46.544	400	1025	246	1771	424	104	27	392	106	87	23	30	8	76	19	10	3	59	14	11	3	32	9	4	1	28	7	3	1	610	145	396756	100712	44	10
21	-19.6724	46.544	500	861	211	1659	406	173	45	648	166	136	34	39	10	111	27	35	10	90	26	17	4	46	12	6	2	40	10	6	1	1167	290	545340	138414	142	34
21	-19.6724	46.544	600	1681	410	3232	773	222	54	737	182	90	23	23	6	88	22	15	4	73	19	15	4	40	10	6	2	37	9	5	1	744	181	437179	107335	72	18
21	-19.6724	46.544	700	1085	270	2095	514	280	71	1152	284	463	115	64	16	184	45	25	7	139	38	25	6	68	18	10	3	58	14	8	2	1152	286	383423	98248	135	33
21	-19.6724	46.544	800	807	197	2185	527	138	35	524	127	113	31	30	8	97	24	13	4	79	20	15	4	42	11	6	2	37	9	5	1	1015	251	319133	80422	73	18
21	-19.6724	46.544	1000	1009	251	1947	478	260	66	1029	266	215	58	59	15	171	42	25	7	129	35	23	6	63	17	9	2	54	13	7	2	1074	266	356247	91284	125	31
21	-19.6724	46.544	1200	533	131	1359	334	120	31	446	111	89	23	20	5	81	20	11	3	68	19	13	3	37	9	5	1	35	9	4	1	678	169	242175	61178	79	19
26	-22.6046	50.278	20	986	301	642	194	163	50	610	185	126	43	85	29	307	98	82	29	253	89	49	16	144	54	20	7	136	44	21	7	2056	625	1047038	312975	48	16
26	-22.6046	50.278	50	2314	763	1354	437	384	133	1520	492	316	118	85	29	307	98	82	29	253	89	49	16	144	54	20	7	136	44	21	7	2875	969	1921230	664857	72	23
26	-22.6046	50.278	75	881	270	952	288	167	53	640	195	122	42	35	12	125	38	23	6	104	33	21	6	60	19	8	3	58	14	8	2	1241	379	362303	112652	58	18
26	-22.6046	50.278	99	545	167	347	109	97	30	369	115	77	25	19	6	90	30	11	4	63	21	13	4	36	12	5	2	33	10	4	1	720	226	159261	49282	30	9
26	-22.6046	50.278	200	351	108	567	174	49	15	190	60	42	15	10	3	49	17	7	2	37	13	7	2	19	6	3	1	18	6	2	1	504	158	423971	134490	32	10
26	-22.6046	50.278	400	409	124	769	232	73	24	283	89	54	19	21	7	56	17	8	3	47	15	9	3	27	9	4	1	23	7	3	1	578	180	404037	127470	42	13
26	-22.6046	50.278	599	452	141	1589	488	99	31	360	111	82	26	23	8	72	22	11	3	61	19	12	4	33	11	5	2	31	10	4	1	688	213	356914	112263	44	14
26	-22.6046	50.278	800	651	199	1777	539	129	40	508	157	103	34	29	9	92	28	14	4	74	24	14	4	39	11	5	1	29	9	3	1	717	216	366424	114813	73	22
26	-22.6046	50.278	1000	492	147	1557	463	104	33	407	126	86	28	29	9	79	24	11	4	62	19	12	4	34	11	5	2	36	11	4	1	667	200	300224	96007	64	19
32	-26.7030	55.515	10	1263	302	687	160	215	56	822	195	162	42	38	9	165	38	23	6	143	35	29	7	87	23	13	4	84	20	13	3	1651	385	80348	19906	44	10
32	-26.7030	55.515	20	3478	1043	1456	433	447	147	1712	508	344	92	79	24	345	142	51	19	320	110	66	19	200	73	29	12	196	58	30	9	4200	1177	203072	60179	71	20

https://doi.org/10.5194/bg-2019-462
Preprint. Discussion started: 7 January 2020

Biogeosciences
Discussions
Open Access
EGU

Station	Longitude	Latitude	Depth [m]	La	2σ	Ce	2σ	Pr	2σ	Nd	2σ	Sm	2σ	Eu	2σ	Gd	2σ	Tb	2σ	Dy	2σ	Ho	2σ	Er	2σ	Tm	2σ	Yb	2σ	Lu	2σ	Y	2σ	Ba	2σ	Th	2σ
32	-26.7030	55.515	40	1142	271	751	178	200	51	754	186	154	42	35	6	154	36	23	6	141	37	29	7	90	23	13	3	91	21	14	3	1632	398	101837	25144	53	13
32	-26.7030	55.515	60	593	145	398	96	112	29	426	108	89	25	21	4	90	22	13	4	79	21	16	4	48	13	7	2	47	11	6	2	851	212	105418	26265	34	8
32	-26.7030	55.515	80	827	213	606	153	144	40	545	141	119	38	27	7	108	27	14	4	84	25	16	4	43	12	6	2	38	10	5	1	880	232	113079	30251	28	8
32	-26.7030	55.515	100	627	150	362	85	119	30	426	101	90	25	21	5	85	20	12	3	67	18	13	3	35	10	4	1	32	7	4	1	762	180	140814	35351	23	6
32	-26.7030	55.515	120	558	140	403	100	89	23	337	85	75	20	18	5	71	18	9	2	60	17	12	3	32	9	5	1	30	8	4	1	704	178	311306	78820	31	8
32	-26.7030	55.515	140	381	92	2518	602	70	17	273	67	60	13	8	2	44	11	6	2	48	13	10	3	31	9	3	1	25	6	3	1	691	165	277244	72189	29	7
32	-26.7030	55.515	161	649	158	896	218	89	22	335	84	70	18	8	2	71	17	33	9	48	13	10	3	27	8	4	1	25	6	3	1	574	145	418735	106021	55	13
32	-26.7030	55.515	200	312	72	432	99	50	12	192	45	47	11	13	3	39	10	6	1	35	8	5	2	21	6	3	1	20	5	2	1	460	125	646966	180885	124	31
32	-26.7030	55.515	300	589	140	1143	269	101	25	375	90	70	21	26	7	69	16	13	4	58	15	11	3	31	8	4	1	28	7	3	1	679	157	497786	126347	54	12
32	-26.7030	55.515	380	543	131	975	235	90	23	347	87	68	19	17	4	66	16	12	3	57	16	11	3	31	9	4	1	26	6	3	1	556	137	463739	116271	65	16
32	-26.7030	55.515	450	11425	2812	16272	4695	140	35	428	108	91	22	24	6	99	25	10	3	60	16	12	3	33	9	5	1	31	8	3	1	596	185	590904	142516	60	18
32	-26.7030	55.515	500	545	132	1366	328	108	27	418	103	89	24	23	6	81	20	13	3	64	17	12	3	35	9	5	1	30	7	4	1	612	151	357061	91240	54	13
32	-26.7030	55.515	598	470	111	1201	287	102	25	390	93	72	18	21	5	70	17	10	3	60	16	11	3	32	9	5	1	30	7	4	1	674	161	310797	73879	55	13
32	-26.7030	55.515	700	531	141	1427	373	115	34	418	110	78	21	18	6	71	18	10	3	59	16	11	3	31	9	5	1	29	7	3	1	705	193	282115	76794	55	14
32	-26.7030	55.515	800	578	144	1565	386	115	30	423	104	80	23	27	7	79	19	11	3	63	17	12	3	32	10	4	1	28	7	3	1	590	147	316075	87121	68	17
32	-26.7030	55.515	1000	559	138	1469	365	114	29	442	115	72	20	22	5	82	20	15	4	66	17	13	3	35	10	5	1	34	8	4	1	846	207	262164	68862	56	14
38	-31.2660	58.843	10	4901	1132	6127	1419	372	87	1393	328	247	58	57	14	274	72	33	8	188	45	36	9	100	24	12	3	76	18	9	2	2166	503	196968	46599	37	9
38	-31.2660	58.843	20	2725	607	1704	379	504	112	2535	564	355	79	80	18	420	94	48	11	271	61	52	12	138	31	18	4	110	25	14	3	2957	654	100956	22479	40	9
38	-31.2660	58.843	40	1667	398	1095	259	345	86	1276	303	244	64	54	13	217	55	30	8	169	44	31	7	87	22	11	3	67	16	9	2	1826	430	184356	46234	135	34
38	-31.2660	58.843	60	609	145	358	90	125	32	477	116	99	24	21	5	84	27	11	3	68	17	12	3	32	8	5	1	26	6	2	1	682	167	115360	27528	111	27
38	-31.2660	58.843	80	437	103	478	115	72	17	274	67	56	15	13	3	54	13	7	2	43	12	8	2	22	6	3	1	20	5	2	1	367	88	176560	44333	18	5
38	-31.2660	58.843	100	378	91	3169	751	68	17	252	61	51	14	13	3	50	12	7	2	40	11	8	2	22	6	3	1	20	5	2	1	336	83	249864	61826	20	5
38	-31.2660	58.843	120	410	101	543	133	68	17	252	63	56	16	15	4	53	13	7	2	42	12	8	2	21	6	3	1	19	5	2	0	416	104	357124	90658	60	15
38	-31.2660	58.843	140	454	109	563	135	68	16	262	64	50	15	13	3	53	12	8	2	46	11	9	2	25	7	4	1	23	5	3	1	389	97	498773	119718	23	6
38	-31.2660	58.843	160	751	183	1144	275	108	27	417	105	79	21	23	6	77	19	11	3	62	17	12	3	34	9	5	1	31	8	4	1	658	163	635890	162463	108	29
38	-31.2660	58.843	180	492	117	547	129	91	19	310	74	69	17	15	4	75	22	10	2	55	14	11	3	31	8	4	1	27	7	3	1	504	121	644843	154930	31	7
38	-31.2660	58.843	200	468	109	599	142	85	20	334	79	67	18	16	4	66	16	16	4	57	14	11	3	29	8	4	1	27	7	3	1	516	131	595067	145273	26	7
38	-31.2660	58.843	300	578	142	1022	251	120	31	477	121	102	28	37	10	98	24	15	4	82	22	16	4	44	12	6	2	38	10	4	1	749	194	745823	188037	52	13
38	-31.2660	58.843	400	865	214	1615	398	197	50	769	198	146	41	51	13	154	39	23	6	132	34	25	6	68	19	9	2	57	14	7	2	1338	340	679261	173766	68	18
38	-31.2660	58.843	500	834	202	1652	401	200	50	816	202	185	49	52	13	197	52	26	7	151	36	28	7	78	20	10	3	65	16	8	2	1420	346	428812	108888	63	17
38	-31.2660	58.843	600	1145	274	2292	544	241	61	980	247	205	59	70	18	203	49	32	8	175	45	33	8	91	24	12	3	77	18	10	2	1540	378	525323	133169	107	26
38	-31.2660	58.843	700	931	218	1782	423	196	46	802	192	239	57	45	10	160	37	25	6	138	32	26	6	74	19	9	2	62	15	8	2	1421	336	732581	178220	80	20
38	-31.2660	58.843	800	2191	530	5086	1249	340	89	1194	288	151	43	38	9	148	36	27	7	124	32	23	6	64	18	8	2	53	13	6	2	1042	259	273012	68519	70	19
38	-31.2660	58.843	1000	896	216	1774	421	238	60	969	245	208	54	56	13	208	50	32	9	178	44	33	8	90	24	12	3	75	18	9	2	1523	368	244631	62115	84	21
44	-38.954	59.62	10	719	169	592	136	121	29	445	105	89	22	25	6	115	26	25	6	129	36	29	7	100	27	17	5	138	31	21	5	1911	455	115394	24301	82	20
44	-38.954	59.62	20	823	191	477	110	131	32	564	145	97	23	29	7	127	30	21	5	153	38	35	8	123	32	21	6	172	38	27	6	2496	576	95415	20162	82	19
44	-38.954	59.62	40	545	128	476	111	109	26	436	101	94	22	25	6	101	23	20	5	92	22	19	4	56	14	8	2	57	13	8	2	1242	298	282420	65571	48	11
44	-38.954	59.62	60	792	184	799	186	107	25	386	90	86	20	20	5	87	20	12	3	75	17	15	3	44	11	6	2	44	10	5	1	787	189	287476	65939	40	9
44	-38.954	59.62	80	394	87	911	202	80	18	293	64	64	14	15	3	60	13	8	2	49	12	9	2	28	7	4	1	25	6	3	1	770	175	432487	95159	42	9
44	-38.954	59.62	100	456	110	716	174	93	23	336	82	64	16	20	7	65	16	9	2	55	14	11	3	30	8	4	1	27	6	3	1	540	138	428979	104464	41	10
44	-38.954	59.62	120	384	84	1813	395	84	19	303	67	67	15	15	3	63	14	9	2	54	13	10	2	29	7	4	1	26	6	3	1	501	114	436440	95418	36	8
44	-38.954	59.62	140	402	93	608	140	85	20	307	71	67	15	25	6	65	15	8	2	49	12	9	2	26	6	3	1	23	5	2	1	557	136	435327	99893	34	8
44	-38.954	59.62	160	1739	409	3254	765	122	29	402	95	73	17	18	4	78	18	n.d.	n.d.	57	14	11	2	31	8	4	1	26	6	3	1	545	134	517949	123930	44	10
44	-38.954	59.62	200	665	145	1155	253	140	31	488	108	95	22	18	4	84	19	12	3	64	14	12	3	33	8	4	1	28	6	3	1	582	132	663764	144442	38	8
44	-38.954	59.62	300	505	112	1082	239	112	25	395	87	82	19	21	5	76	17	12	3	64	14	12	3	34	8	4	1	25	6	3	1	685	155	715076	157662	45	10
44	-38.954	59.62	400	504	112	918	204	111	25	401	88	88	19	21	5	83	20	11	3	62	14	12	3	32	7	4	1	27	6	3	1	603	137	718667	158289	48	10
44	-38.954	59.62	500	603	139	1205	276	128	30	452	104	84	20	26	6	81	18	n.d.	n.d.	66	15	12	3	34	8	5	1	30	7	3	1	654	157	643485	146382	55	12
44	-38.954	59.62	600	577	128	1147	254	127	29	452	100	90	20	19	4	84	20	14	3	57	13	10	2	28	7	4	1	23	5	2	1	423	97	482268	105587	55	12
44	-38.954	59.62	700	473	109	825	190	96	23	336	78	72	17	19	5	67	16	9	2	50	12	9	2	28	6	3	1	21	5	2	0	473	117	657898	149374	41	9
44	-38.954	59.62	800	259	60	471	109	55	13	194	45	43	10	10	2	36	9	6	2	28	7	5	1	15	4	2	1	13	3	1	0	201	52	484902	111536	28	7
44	-38.954	59.62	1100	573	126	1394	306	125	28	431	96	86	19	16	4	84	20	14	3	64	16	12	3	34	8	4	1	29	6	3	1	491	114	282183	62238	60	13
44	-38.954	59.62	1401	901	211	1848	436	142	34	511	126	108	25	46	16	98	23	13	3	78	18	15	4	41	10	6	2	34	8	4	1	1571	373	119978	28695	57	13
51	-42.013	59.8	10	587	137	415	98	102	24	376	88	84	19	20	5	95	22	n.d.	n.d.	102	25	22	5	77	19	13	3	111	26	18	4	1571	373	119978	28695	57	13
51	-42.013	59.8	19	415	90	518	110	57	13	212	46	45	10	11	3	47	10	8	2	54	13	12	3	41	10	7	2	57	12	9	2	707	153	61431	13153	33	8
51	-42.013	59.8	40	607	143	497	118	101	24	371	88	84	19	20	5	88	21	13	3	85	22	17	4	55	14	8	2	66	15	10	2	1157	282	166379	40182	38	9
51	-42.013	59.8	60	636	145	490	113	100	25	497	121	84	19	20	5	81	24	12	3	82	21	17	4	50	13	8	2	57	13	8	2	1011	242	179071	42593	49	11
51	-42.013	59.8	80	653	148	1497	340	110	29	421	113	91	25	22	5	84	19	12	3	71	17	13	3	38	10	6	2	39	9	5	1	807	191	242637	58355	50	12
51	-42.013	59.8	100	726	162	1113	253	131	30	460	105	91	20	22	5	88	21	17	4	72	17	14	3	39	11	6	1	40	9	5	1	828	192	298481	67616	48	11
51	-42.013	59.8	120	574	133	1387	320	145	34	524	120	104	24	31	7	103	23	14	3	86	20	16	4	43	11	6	1	36	9	4	1	896	214	185884	42526	62	14
51	-42.013	59.8	140	764	174	1444	330	156	37	555	127	111	26	26	6	106	26	13	3	81	20	15	4	43	10	6	1	38	9	4	1	790	188	279389	63794	65	15
51	-42.013	59.8	160	667	155	1350	312	151	35	533	123	103	24	25	6	105	25	14	3	75	18	14	3	38	9	5	1	34	8	4	1	722	175	261005	59758	66	15
51	-42.013	59.8	180	925	209	1833	411	206	47	728	163	143	32	34	8	126	28	17	4	101	24	18	4	52	12	7	2	45	10	5	1	926	215	248305	55961	88	20
51	-42.013	59.8	200	1105	259	2306	539	247	59	888	223	172	45	45	12	201	61	25	7	131	37	24	6	68	19	9	2	58	15	7	2	1193	295	350485	83561	110	27
51	-42.013	59.8	300	1358	295	2470	539	142	32	539	119	89	22	29	9	101	22	15	3	86	19	17	4	46	10	6	1	40	9	5	1	918	203	462097	99867	78	17
51	-42.013	59.8	400	1045	246	2107	494	231	54	826	193	165	38	41	10	165	39	21	5	131	31	24	6	67	16	9	2	59	14	7	2	1786	431	426025	99616	87	20
51	-42.013	59.8	500	1061	229	2598	562	279	62	1029	223	208	45	54	12	192	46	27	6	159	35	29	6	81	19	11	2	67	14	8	2	1436	317	321786	69981	108	23

https://doi.org/10.5194/bg-2019-462
Preprint. Discussion started: 7 January 2020

Biogeosciences
Discussions
Open Access
EGU

Station	Longitude	Latitude	Depth [m]	La	2σ	Ce	2σ	Pr	2σ	Nd	2σ	Sm	2σ	Eu	2σ	Gd	2σ	Tb	2σ	Dy	2σ	Ho	2σ	Er	2σ	Tm	2σ	Yb	2σ	Lu	2σ	Y	2σ	Ba	2σ	Th	2σ
51	-42.013	59.8	600	444	103	1018	235	105	24	385	88	76	18	25	6	77	17	11	3	65	15	12	3	34	8	5	1	28	7	3	1	926	222	225811	52006	40	9
51	-42.013	59.8	700	503	120	1172	268	117	27	431	102	153	34	20	6	88	20	12	3	74	17	14	3	40	10	6	1	37	9	5	1	866	217	259060	59188	50	12
51	-42.013	59.8	800	737	161	2256	492	201	46	729	161	153	36	36	8	143	31	21	5	119	28	22	5	61	14	8	2	51	11	6	1	1125	254	229489	51043	73	15
51	-42.013	59.8	1000	530	123	1280	295	134	31	484	111	96	22	29	7	95	22	13	3	79	18	14	3	40	10	5	1	33	8	4	1	827	197	171596	39258	57	13
53	-43.006	59.9	10	4261	975	8331	1915	1178	272	3883	887	669	152	152	35	540	122	73	18	426	101	77	18	218	54	30	7	211	48	30	7	5376	1250	334887	77894	557	128
53	-43.006	59.9	20	6231	1442	12578	2920	1763	414	5523	1278	902	207	180	41	693	158	95	23	520	125	95	22	272	66	39	9	278	63	39	9	6246	1698	254567	60201	1145	262
53	-43.006	59.9	40	3420	798	5684	1329	712	169	2364	550	408	94	94	22	317	74	44	10	246	61	44	10	125	31	17	4	117	27	16	4	2765	660	156732	37092	360	84
53	-43.006	59.9	60	3995	860	8782	1884	1039	225	3402	730	562	120	125	27	438	94	58	13	321	71	56	12	152	34	20	4	128	28	17	4	3358	729	149072	32434	455	101
53	-43.006	59.9	80	5235	1161	11362	2508	1413	316	4472	993	725	158	158	36	535	118	67	15	385	87	67	15	180	42	24	5	152	33	20	4	4185	954	136371	34857	648	143
53	-43.006	59.9	100	5446	1246	11499	2655	1503	352	4755	1101	772	177	174	40	581	133	74	18	422	101	75	17	204	51	27	6	177	41	23	5	4434	1044	268511	63558	655	154
53	-43.006	59.9	120	4022	938	7634	1785	973	232	3268	763	563	131	130	30	454	105	59	14	341	81	61	14	170	41	23	6	156	36	21	5	3709	889	303677	72584	448	106
53	-43.006	59.9	140	6849	1498	14593	3160	1962	435	6077	1315	932	199	208	45	678	147	86	19	459	109	80	17	221	52	28	7	185	40	24	5	5209	1145	198138	43745	963	214
64	-46.083	59.07	10	165	39	201	48	27	7	90	22	18	4	4	1	19	5	3	1	18	5	4	1	12	3	2	0	15	4	2	0	272	70	52388	12757	20	6
64	-46.083	59.07	20	496	117	677	162	60	14	198	48	33	8	6	2	35	8	6	2	84	20	15	4	42	11	6	2	38	9	4	1	727	181	369040	87600	66	15
64	-46.083	59.07	40	321	77	307	74	44	11	154	37	37	7	6	2	31	8	4	1	27	7	5	1	16	4	2	0	16	4	2	0	292	75	74615	17889	19	5
64	-46.083	59.07	60	395	93	295	70	44	13	148	37	37	8	10	3	40	11	6	2	29	8	6	2	20	6	3	1	17	4	2	0	n.d.	n.d.	86258	21579	29	8
64	-46.083	59.07	80	335	79	338	80	45	11	203	49	48	11	10	3	63	14	8	2	36	9	8	2	20	6	4	1	20	5	3	1	0	n.d.	138279	31523	32	8
64	-46.083	59.07	100	2796	614	3978	1062	231	49	750	165	59	13	13	3	63	14	8	2	48	11	9	2	27	6	3	1	24	5	3	1	336	73	214724	48160	34	8
64	-46.083	59.07	120	652	152	1165	268	105	24	384	87	84	19	21	5	80	18	12	3	68	16	13	3	39	10	5	1	34	8	4	1	718	166	353753	80489	44	10
64	-46.083	59.07	140	551	133	4264	1032	111	27	391	94	79	19	20	5	86	21	11	3	68	17	13	3	39	10	6	1	38	9	5	1	650	165	400624	97051	56	13
64	-46.083	59.07	160	707	167	1388	326	155	37	562	133	116	27	27	6	100	23	16	4	84	20	15	4	42	11	6	2	38	9	4	1	727	181	369040	87600	66	15
64	-46.083	59.07	180	1221	266	2114	463	244	54	948	208	195	46	45	10	170	39	31	7	141	32	27	6	73	18	10	2	64	14	8	2	1341	299	485672	105654	120	26
64	-46.083	59.07	200	1148	278	2470	577	257	60	936	225	176	42	46	11	170	40	23	6	139	34	26	6	71	18	10	2	60	14	7	2	1658	417	369725	86297	110	26
64	-46.083	59.07	300	1122	261	2677	619	301	70	1090	251	213	48	50	12	182	42	25	6	141	33	26	6	71	17	9	2	59	14	7	2	1366	323	265722	62206	125	29
64	-46.083	59.07	400	595	144	1064	248	128	30	453	108	87	21	22	5	84	20	11	3	69	17	13	3	36	9	5	1	30	7	3	1	568	148	495673	114734	51	12
64	-46.083	59.07	600	612	146	1091	249	133	37	484	117	101	26	0	0	93	21	11	3	77	22	15	3	36	9	6	2	32	8	4	1	953	225	478865	114583	65	15
64	-46.083	59.07	700	467	114	1089	254	109	25	387	93	52	15	19	5	75	17	10	3	60	15	11	3	31	8	4	1	25	6	2	1	480	126	351230	81857	47	11
64	-46.083	59.07	800	644	142	1349	298	148	33	522	115	104	23	25	6	96	21	13	3	78	18	14	3	40	9	5	1	35	8	4	1	714	163	619258	137486	65	14
64	-46.083	59.07	900	633	142	1454	325	158	36	563	126	111	25	27	6	102	22	14	3	82	19	15	3	41	10	5	1	34	8	5	1	679	159	516497	114976	65	14
64	-46.083	59.07	1000	595	131	1194	263	128	29	455	100	89	20	22	5	82	18	n.d.	n.d.	65	9	12	3	34	8	5	1	28	6	3	1	579	133	473878	104268	55	12
69	-48.093	55.84	11	1105	237	1378	299	153	35	617	137	115	25	26	6	102	23	13	3	80	18	15	3	42	10	6	1	38	8	5	1	856	201	291504	63034	85	19
69	-48.093	55.84	20	1974	403	1446	296	134	30	482	104	113	34	26	6	115	26	25	5	126	29	28	6	93	24	14	3	124	26	18	4	1666	191	172949	36250	101	21
69	-48.093	55.84	41	588	130	875	192	93	21	319	70	62	14	14	3	58	13	8	2	50	11	9	2	29	7	4	1	30	7	4	1	696	162	145430	32213	50	11
69	-48.093	55.84	60	1058	235	1523	325	114	25	393	87	80	17	17	4	68	15	11	2	55	12	11	2	30	7	4	1	29	6	3	1	637	149	159592	33892	54	12
69	-48.093	55.84	80	891	201	2992	645	180	39	617	137	115	25	26	6	102	23	13	3	80	18	15	3	42	10	6	1	38	8	5	1	856	201	291504	63034	85	19
69	-48.093	55.84	100	970	209	1595	340	159	35	583	125	113	30	29	6	102	21	16	4	80	22	15	3	44	11	6	2	40	8	5	1	909	194	399717	90244	91	19
69	-48.093	55.84	120	1134	253	1982	440	195	44	667	148	125	28	29	6	108	24	15	3	88	20	16	4	45	11	6	1	40	9	5	1	1180	275	401283	88829	95	21
69	-48.093	55.84	140	1118	231	1944	386	205	43	780	173	146	31	35	9	128	31	25	6	99	24	19	4	51	12	3	1	39	8	5	1	1117	231	437093	92096	105	22
69	-48.093	55.84	200	842	172	1563	319	166	35	562	117	103	21	23	5	87	18	11	2	69	15	13	3	35	8	5	1	31	6	3	1	900	191	509727	105738	76	15
69	-48.093	55.84	300	749	158	1236	260	131	28	486	104	91	21	25	6	81	17	11	2	65	15	12	3	34	8	5	1	30	6	3	1	789	167	582584	124324	72	16
69	-48.093	55.84	400	637	141	1374	291	149	32	516	113	96	22	24	5	86	18	12	3	65	15	12	3	33	8	5	1	29	6	3	1	818	190	542261	115183	87	19
69	-48.093	55.84	502	700	144	1317	269	127	26	466	95	88	21	19	4	76	16	10	2	59	13	11	2	32	7	4	1	26	6	3	1	657	135	577098	119896	64	13
69	-48.093	55.84	601	696	156	1442	311	142	31	487	108	80	19	22	5	78	17	11	2	63	14	12	3	33	8	5	1	29	6	3	1	619	147	642915	137872	59	13
69	-48.093	55.84	700	625	130	1483	306	147	31	510	105	93	20	21	4	83	17	11	3	66	14	12	2	34	7	4	1	29	6	3	1	806	172	637841	133101	67	14
69	-48.093	55.84	802	740	162	1696	370	171	38	604	132	98	20	20	4	99	21	13	3	78	18	14	3	40	9	5	1	33	7	4	1	912	207	629344	135693	82	17
69	-48.093	55.84	900	826	183	1731	384	171	40	594	143	94	24	24	9	91	22	15	4	71	19	13	3	37	10	5	1	31	8	5	1	687	164	505081	112655	87	50
69	-48.093	55.84	1001	623	134	1281	275	136	30	458	99	88	19	23	5	76	16	10	2	60	13	11	2	30	7	4	1	25	5	3	1	603	137	505532	107013	66	14
69	-48.093	55.84	1500	822	171	2068	427	201	42	712	149	126	27	26	6	103	21	13	3	75	16	13	3	35	8	5	1	30	6	3	1	773	165	403509	85000	107	22
69	-48.093	55.84	1501	741	153	1604	330	149	31	518	106	96	20	21	4	98	23	11	3	67	14	12	3	33	8	4	1	28	6	3	1	872	184	381928	78251	66	13
77	-51.095	52.99	10	1755	381	1217	260	157	36	618	135	138	30	29	6	134	30	20	5	131	30	29	6	95	22	15	4	114	25	17	4	1235	280	102841	22007	57	13
77	-51.095	52.99	20	1561	346	781	169	166	37	608	136	144	33	37	8	154	34	23	6	151	35	33	7	110	26	17	4	129	28	19	4	1682	389	108338	23742	59	13
77	-51.095	52.99	39	1663	366	1033	226	253	57	1062	231	242	53	52	11	258	56	33	8	206	47	40	9	130	30	19	4	157	34	15	4	1223	307	150410	33343	82	20
77	-51.095	52.99	60	1081	232	2920	631	196	42	748	162	176	38	38	8	175	38	24	5	149	32	30	6	98	23	16	3	121	26	20	4	2014	442	258705	55333	60	13
77	-51.095	52.99	80	784	180	987	219	144	32	515	117	107	24	24	5	103	23	14	3	87	21	17	4	55	14	8	2	62	14	10	2	659	229	335858	74356	59	13
77	-51.095	52.99	100	919	194	1829	386	182	39	623	132	119	25	25	5	102	22	14	3	84	19	16	3	47	11	7	2	49	10	7	1	1547	330	425425	88597	80	18
77	-51.095	52.99	120	1077	236	1575	339	174	38	610	133	115	27	24	5	85	18	10	2	71	17	14	3	39	9	6	1	37	8	4	1	559	125	347807	76859	85	20
77	-51.095	52.99	140	1087	232	2143	458	200	43	667	144	118	25	24	5	93	20	13	3	71	15	13	3	38	9	5	1	34	7	4	1	657	145	379949	80794	105	24
77	-51.095	52.99	160	995	226	1788	405	193	45	663	162	118	30	24	6	96	26	17	4	71	19	13	3	37	10	6	1	32	8	4	1	555	138	388952	89240	102	25
77	-51.095	52.99	200	1274	277	2709	587	258	56	847	183	146	31	31	7	115	25	16	4	84	19	16	3	44	10	6	1	37	8	4	1	763	170	453521	98941	130	28
77	-51.095	52.99	300	789	176	1736	384	171	39	575	128	104	23	24	5	91	20	11	3	65	15	13	3	34	8	5	1	28	6	3	1	669	156	455819	101375	87	19
77	-51.095	52.99	401	723	163	1619	349	161	36	545	121	96	21	25	6	110	27	11	3	64	14	12	3	32	8	4	1	27	6	3	1	687	163	406978	87730	78	18
77	-51.095	52.99	500	1027	211	2259	467	223	47	746	155	132	27	38	8	101	21	13	3	78	16	14	3	39	9	5	1	33	7	4	1	891	190	491380	102690	107	22
77	-51.095	52.99	601	1627	357	3645	796	199	44	655	145	118	26	25	6	94	21	12	3	69	15	12	3	34	8	5	1	29	6	3	1	558	129	400162	86674	86	20
77	-51.095	52.99	700	992	210	2068	436	218	47	705	151	134	28	28	6	111	23	14	3	85	18	16	3	43	10	6	1	37	8	4	1	754	167	596920	124247	109	23
77	-51.095	52.99	800	677	149	1540	337	166	37	563	123	103	22	24	5	95	21	11	3	61	13	11	2	31	7	4	1	25	5	3	1	508	118	490905	106358	85	19
77	-51.095	52.99	901	1049	217	1920	398	189	40	909	191	167	36	34	7	93	25	13	3	73	15	14	3	37	8	5	1	32	7	3	1	673	148	511759	110480	85	21
77	-51.095	52.99	1002	1807	414	3974	872	166	37	550	124	87	20	29	7	80	18	13	3	63	14	11	3	32	8	4	1	27	6	3	1	554	135	437344	95922	84	19

https://doi.org/10.5194/bg-2019-462
Preprint. Discussion started: 7 January 2020

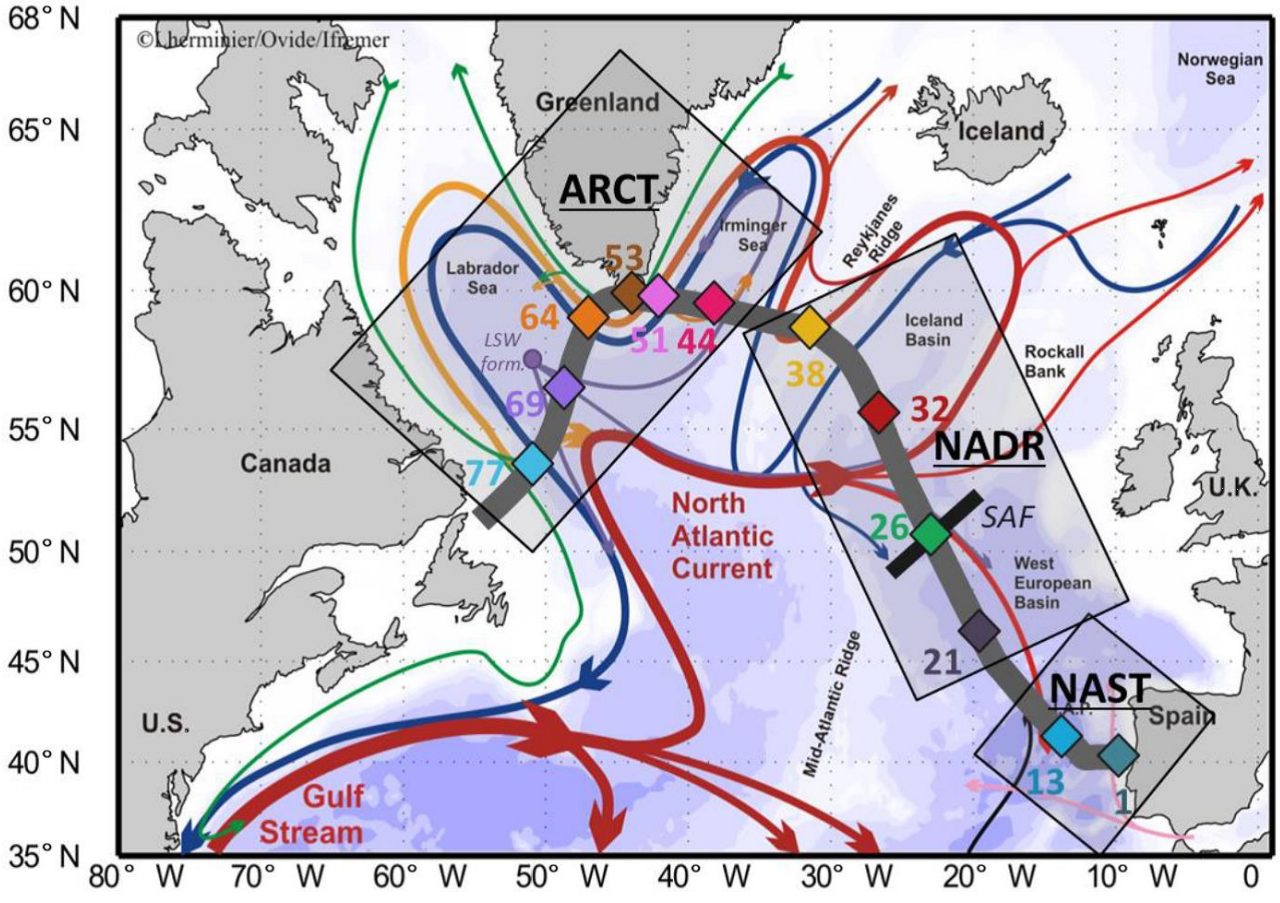

Figure 1: Map of the studied area (Subpolar North Atlantic, SPNA), including schematized circulation features, adapted from García-Ibáñez et al. (2015). Bathymetry is plotted in color with interval boundaries at 100 m, at 1000 m, and every 1000 m below 1000 m. The red and green arrows represent the main surface currents, the pink and orange arrows represent currents at intermediate depths, and the blue and purple arrows represent the deep currents. Diamonds indicate station positions, located in 3 distinct areas (grey squares): the North Atlantic Subtropical province (NAST), the North Atlantic Drift region (NADR), and the Arctic region (ARCT). The approximate locations of the subarctic front (SAF; black bar crossing station #26) and the formation site of the Labrador Sea Water (LSW form.) are indicated. The section used in ODV figures is symbolized by the thick grey line. From Lemaitre et al. (2018).

https://doi.org/10.5194/bg-2019-462
Preprint. Discussion started: 7 January 2020

Biogeosciences Discussions
Open Access
EGU

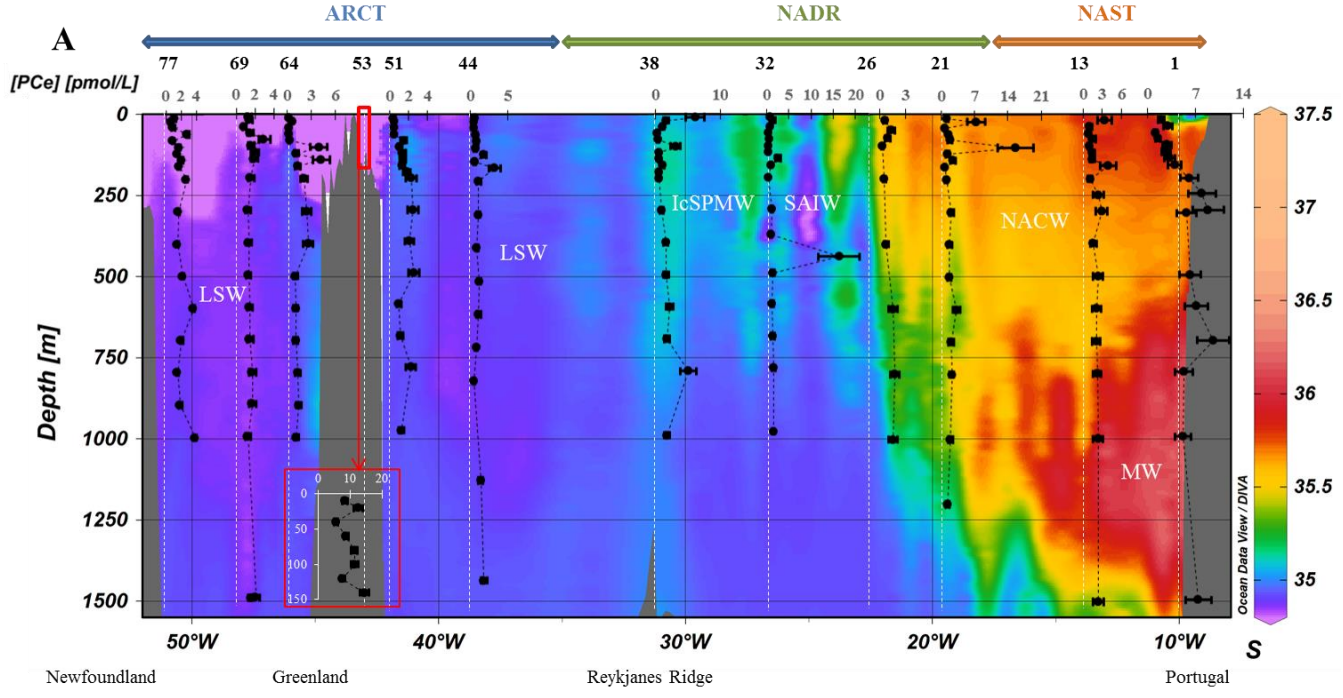

645

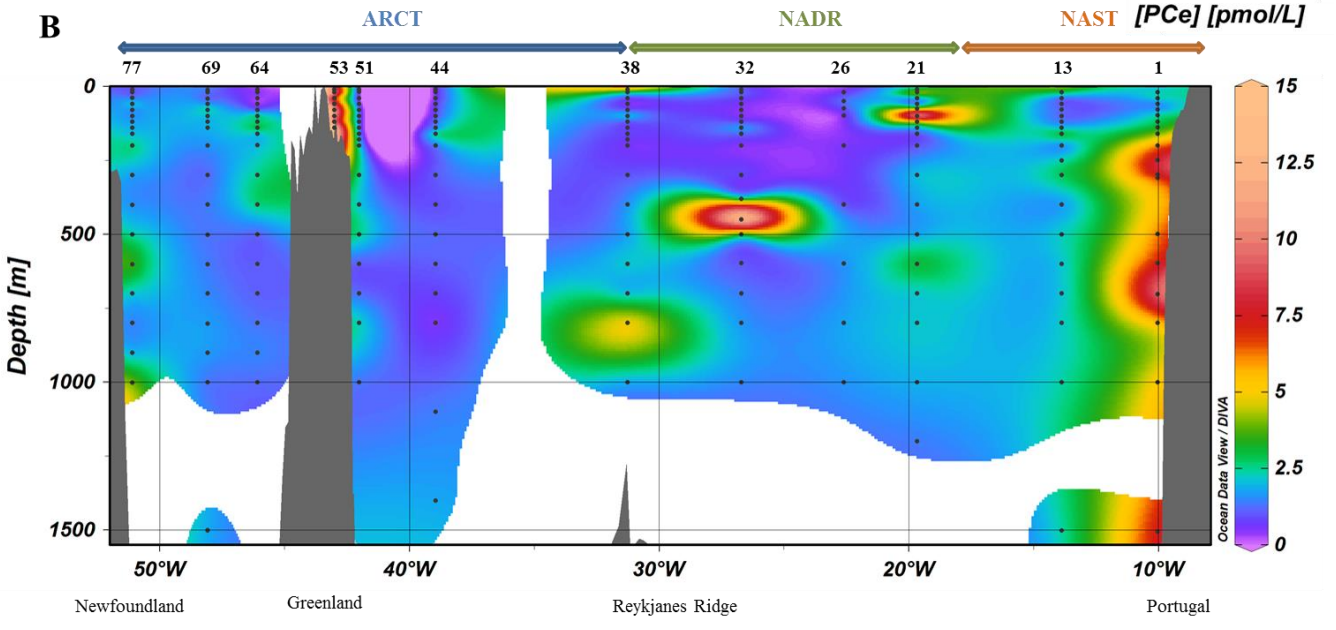

https://doi.org/10.5194/bg-2019-462
Preprint. Discussion started: 7 January 2020

Biogeosciences Discussions Open Access EGU

Figure 2: A. Profiles of particulate [Ce] concentrations superimposed on salinity (S) measured by CTD at every GEOVIDE station (Lherminier and Sarthou, 2017); in white, water masses characterized by a multiparametric (OMP) analysis (García-Ibáñez et al., 2018). For the station #53, profiles are shifted to the bottom at a lower scale because of the shallow depth of the station. This map and the following were created with the software Ocean Data View (Schlitzer, 2016). B. Particulate [Ce] concentrations interpolated with the DIVA gridding function of Ocean Data View along the section defined in Fig. 1.

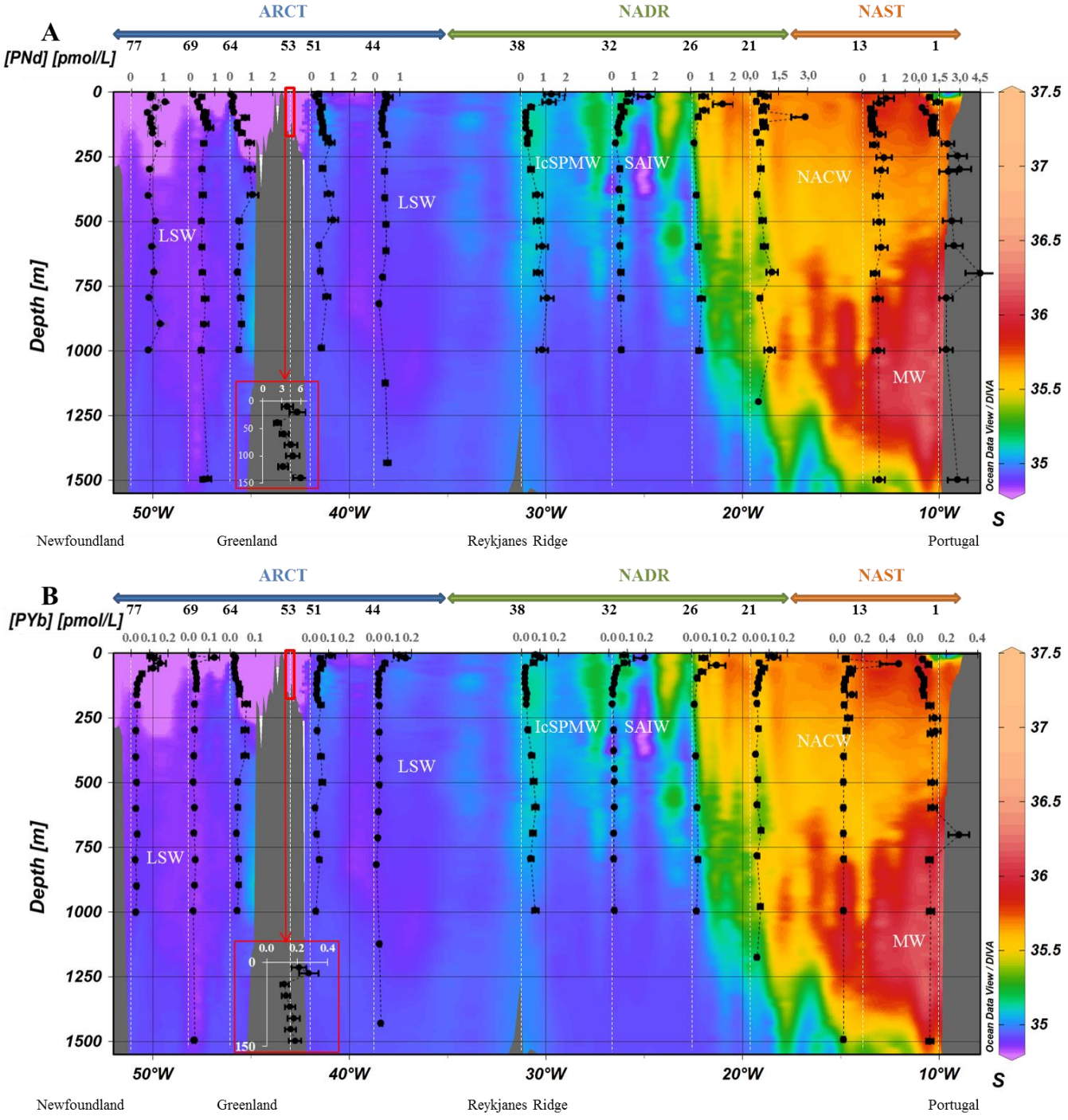

https://doi.org/10.5194/bg-2019-462
Preprint. Discussion started: 7 January 2020

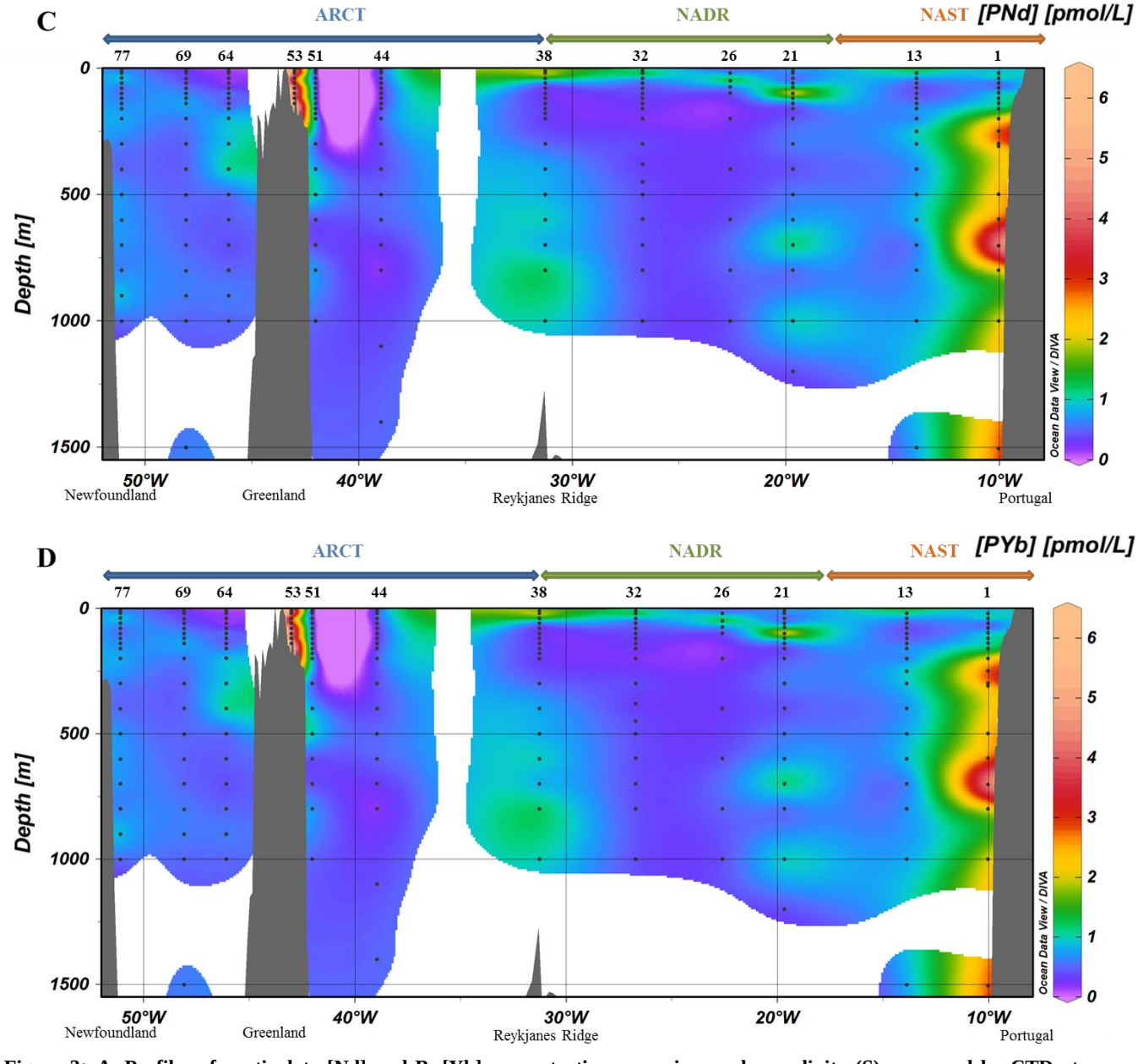

Figure 3: A. Profiles of particulate [Nd] and B. [Yb] concentrations superimposed on salinity (S) measured by CTD at every GEOVIDE station (Lherminier and Sarthou, 2017); in white, water masses characterized by OMP analysis (García-Ibáñez et al., 2018). At station #53, profiles are shifted to the bottom at a lower scale because of the shallow depth of the station. C. Particulate [Nd] and D. [Yb] concentrations interpolated with the DIVA gridding function of Ocean Data View along the section defined in Fig. 1.

https://doi.org/10.5194/bg-2019-462
Preprint. Discussion started: 7 January 2020

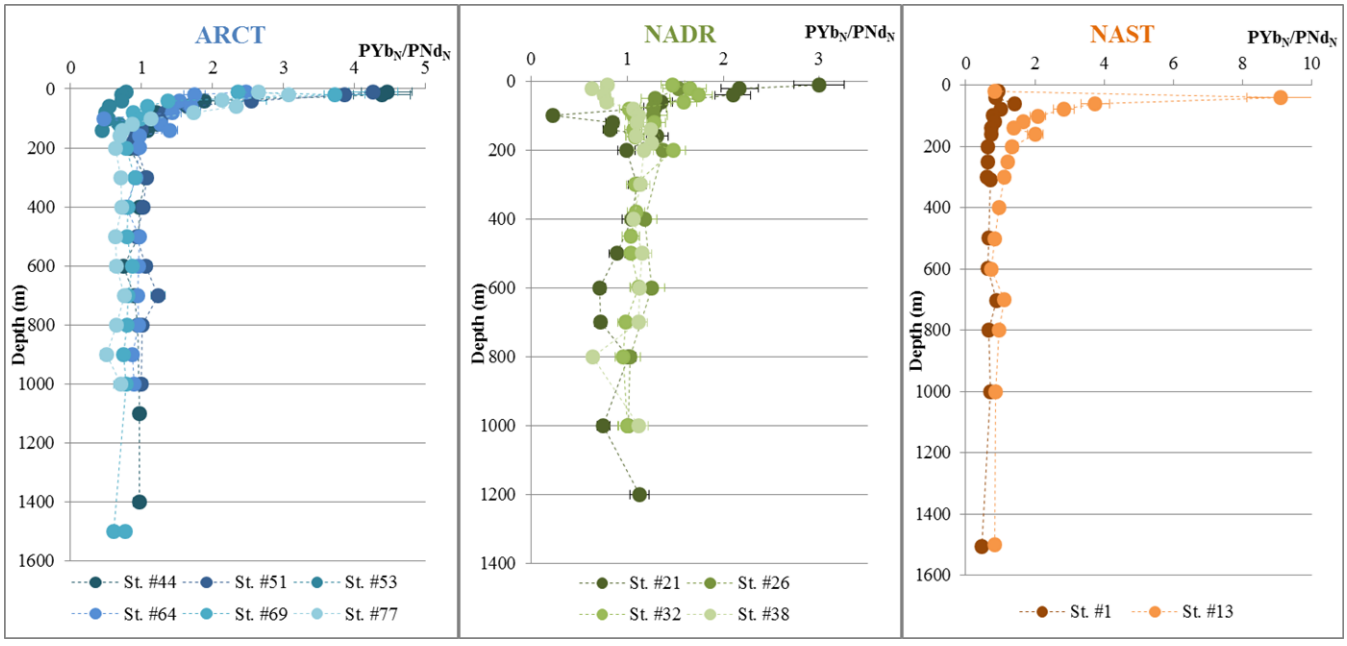

Figure 4: PYb/PNd ratio normalized to PAAS in each biogeochemical province

https://doi.org/10.5194/bg-2019-462
Preprint. Discussion started: 7 January 2020

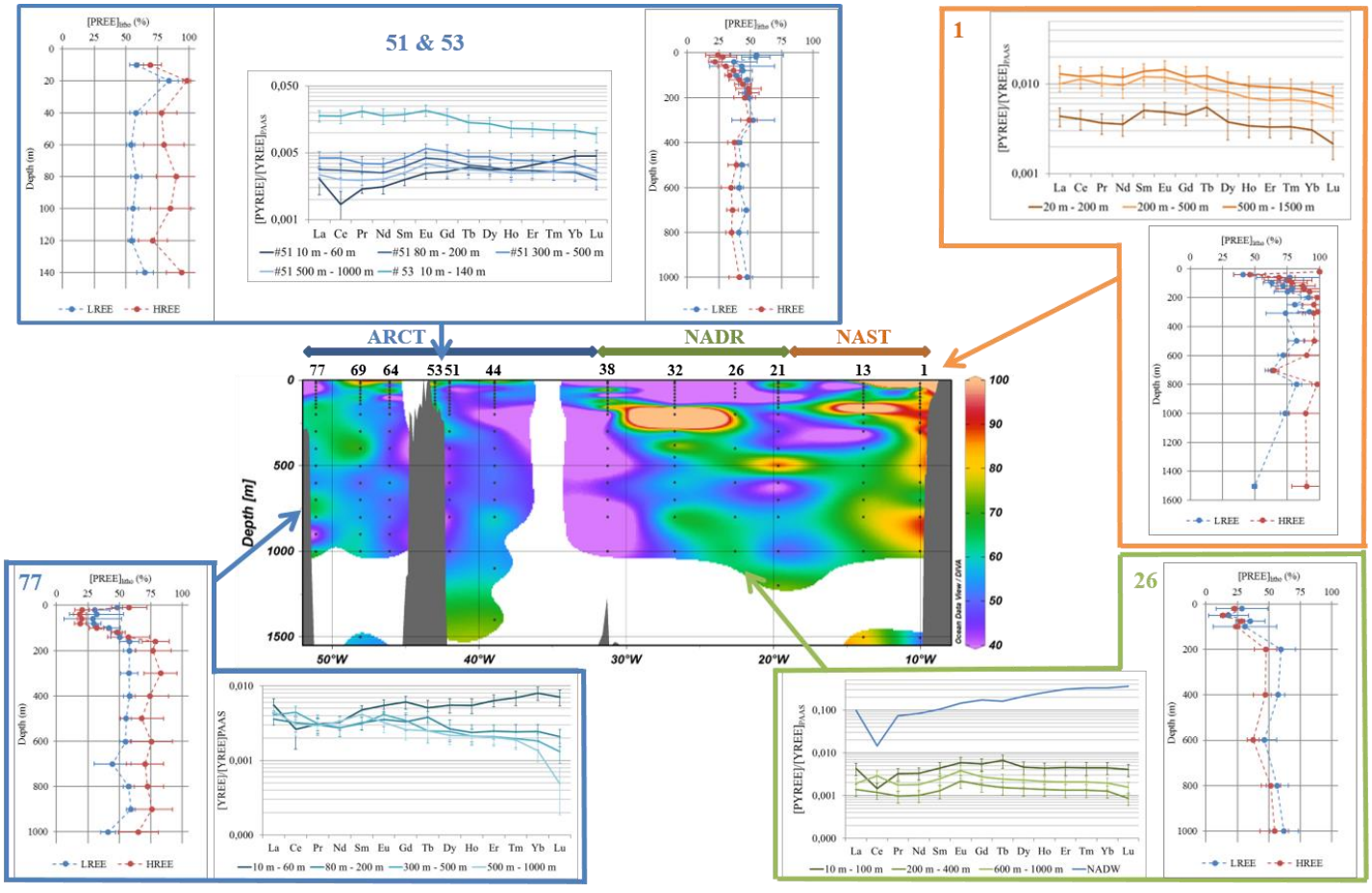

Figure 5: Center: proportion of lithogenic PNd along the GEOVIDE section (in %); Borders: vertical profiles of the lithogenic fraction of LREEs (except Ce, blue lines) and HREEs (red lines) and PAAS-normalized REE patterns of the total fraction, averaged by depth layers, at stations #1, #26, #51, #53 and #77.

https://doi.org/10.5194/bg-2019-462
Preprint. Discussion started: 7 January 2020

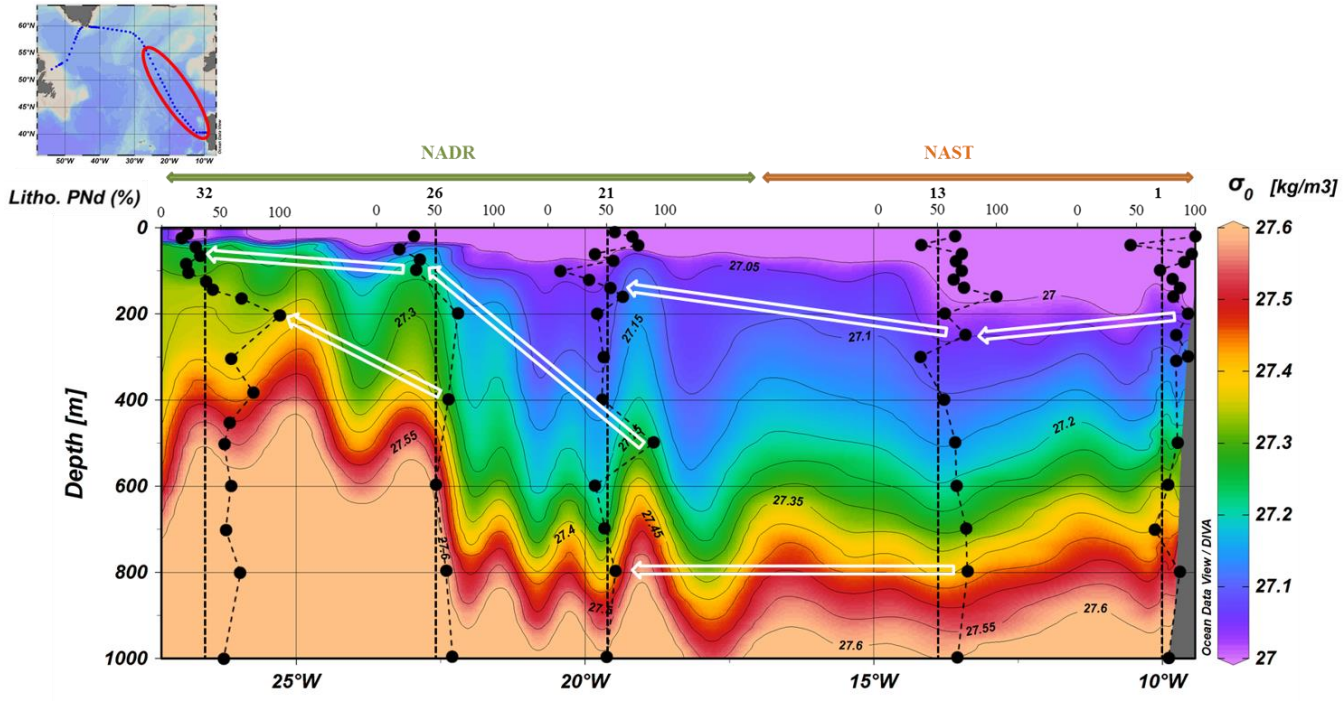

Figure 6: Proportion of lithogenic PNd profiles superposed to density from station #1 to #32

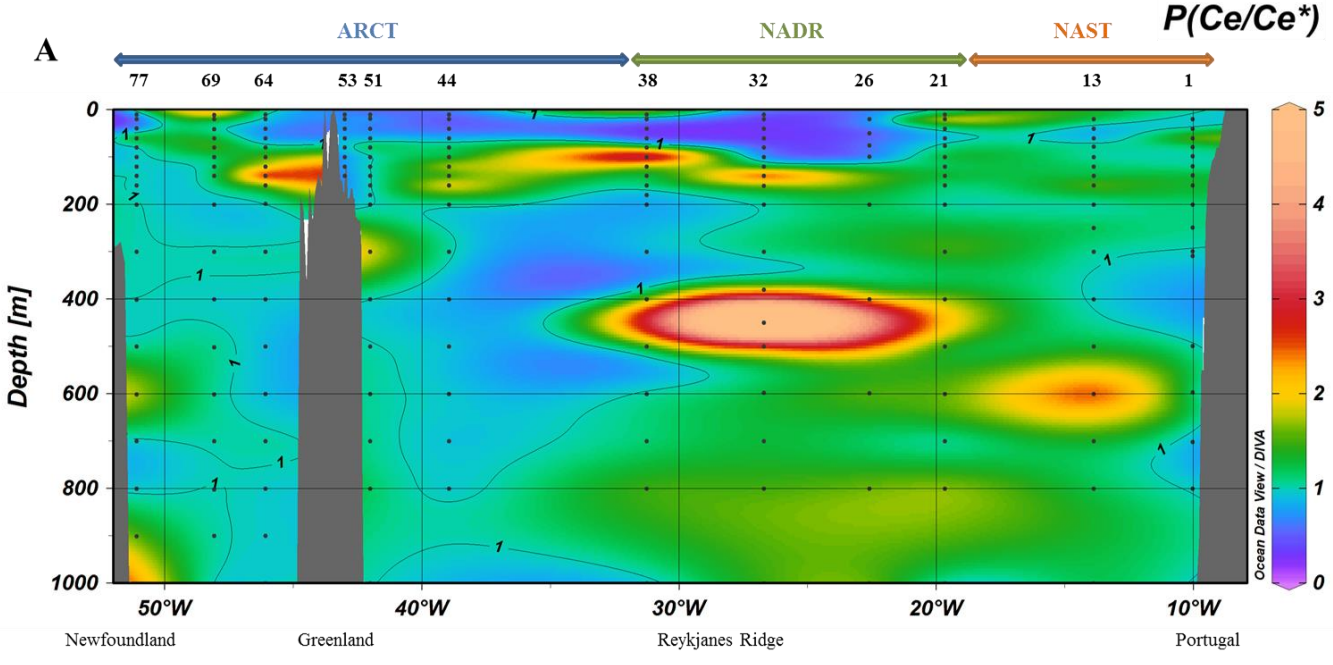

https://doi.org/10.5194/bg-2019-462
Preprint. Discussion started: 7 January 2020

B

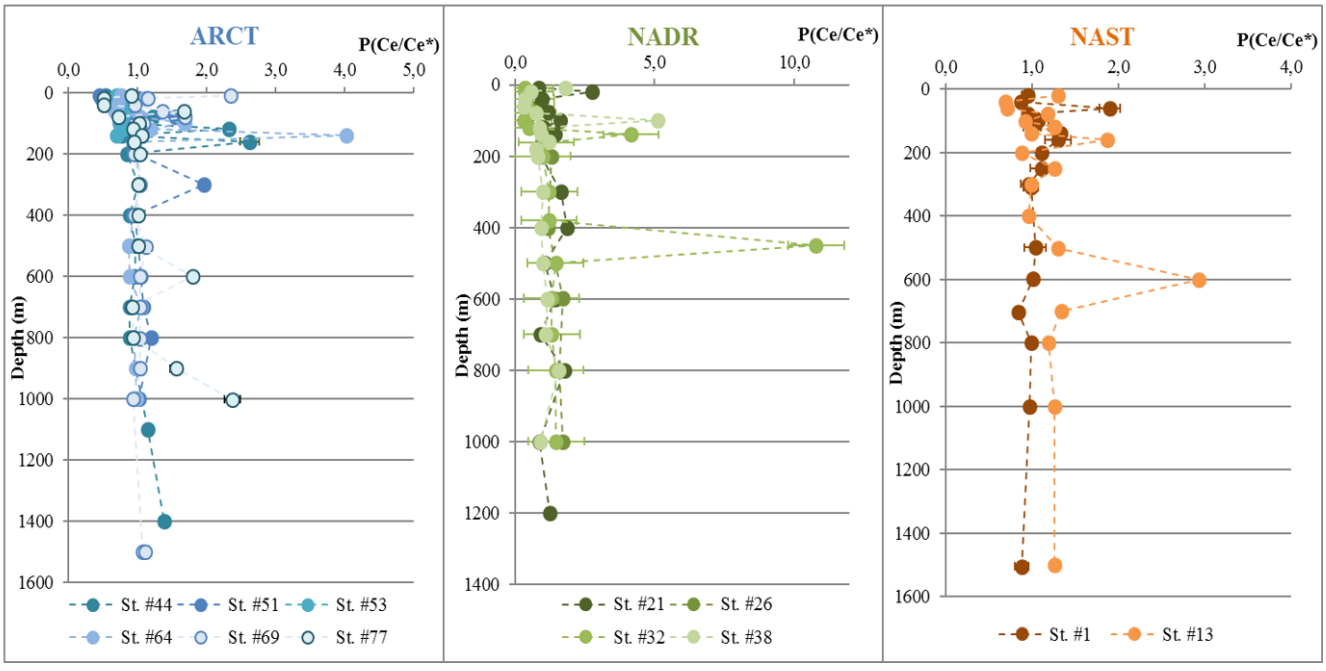

675 **Figure 7: A. Particulate Ce anomaly (Ce/Ce*) along the GEOVIDE section, interpolated with the DIVA gridding function of Ocean Data View and B. Ce/Ce* profiles by biogeochemical provinces.**

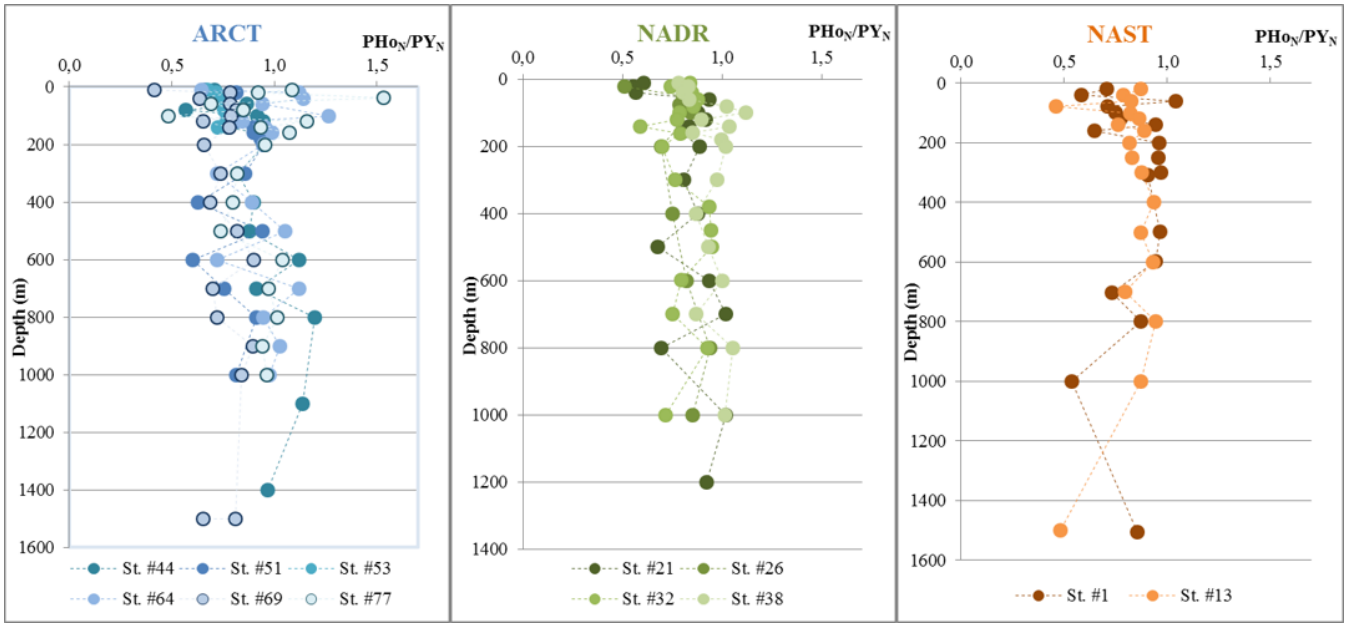

680 **Figure 8: PAAS-normalized PHo/PY profiles by biogeochemical provinces.**

https://doi.org/10.5194/bg-2019-462
Preprint. Discussion started: 7 January 2020

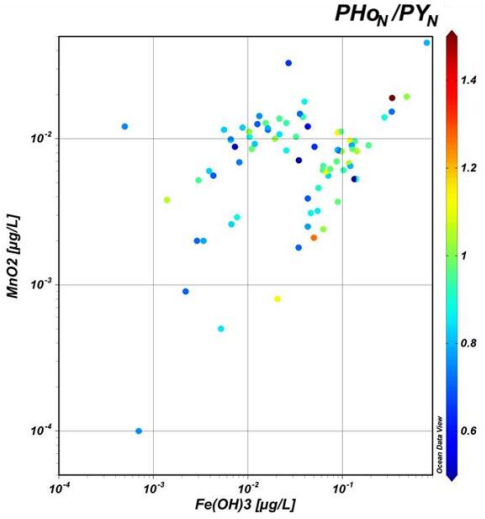

Figure 9: PAAS-normalized PHo/PY ratio as a function of $Fe(OH)_3$ and MnO_2 concentrations (in µg.L^{-1}).

685

Author contribution

N.L. did the sampling during the cruise, helped by C.J. N.L. did the leaching on the filter and first Ba measurements. C.J., M.B., M.G. and M.L. did REE measurements. ML wrote the manuscript, and C.J., H.P., M.G., N.L. and P.L. did the proofreading.

Competing interests

690 The authors declare that they have no conflict of interest.

Acknowledgments

We deeply thank the crew of the N/O Pourquoi Pas who where indispensable for the cruise. We also thank the Dt INSU members for their help. We thank Jérôme Chmeleff, Aurélie Marquet and Camille Duquenoy for their help for the HR-ICP-MS analysis. Many thanks to
695 Michael Bau for his advices on the interpretation of the Y/Ho part. This work was supported by by the French National Research Agency (ANR-13-BS06-0014, ANR-12-PDOC-0025-01), the French National Centre for Scientific Research (CNRS-LEFECYBER, UMR 5566). The logistics was supported by DT-INSU and GENAVIR.